NASA CR 114,531

INVESTIGATION OF BUBBLES IN ARTERIAL HEAT PIPES

by E. W. Saaski
December 1972

Prepared under Contract No. NAS2-6901 by
Donald W. Douglas Laboratories
McDonnell Douglas Astronautics Company
Richland, Washington

for

AMES RESEARCH CENTER
NATIONAL AERONAUTICS AND SPACE ADMINISTRATION

PREFACE

This document is the final report submitted by the Donald W. Douglas Laboratories, a Subdivision of the McDonnell Douglas Astronautics Company, Richland, Washington, under Contract No. NAS2-6991. J. Kirkpatrick was the Technical Manager.

This report covers the period 23 June 1972 through 23 December 1972 and is cataloged as McDonnell Douglas Report MDC G4402.

CONTENTS

FIGURES

TABLES

SUMMARY

The behavior of gas occlusions in arterial heat pipes has been studied experimentally and theoretically. Specifically, the gas-liquid system properties, solubility and diffusivity, have been measured from -50° to 100°C for helium and argon in ammonia, Freon-21 ($CHCl_2F$), and methanol. Properties values obtained were then used to experimentally test models for gas venting from a heat pipe artery under isothermal conditions (i.e., no-heat flow), although the models, as developed, are also applicable to heat pipes operated at power, with some minor modifications. Preliminary calculations indicated arterial bubbles in a stagnant pipe require from minutes to days to collapse and vent.

It has been found experimentally that a gas bubble entrapped within an artery structure has a very long lifetime in many credible situations. This lifetime has an approximately inverse exponential dependence on temperature, and is generally considerably longer for helium than for argon. The models postulated for venting under static conditions were in general quantitative agreement with experimental data. Factors of primary importance in governing bubble stability are artery diameter, artery wall thickness, noncondensible gas partial pressure, and the property group αD (the Ostwald solubility coefficient multiplied by the gas/liquid diffusivity). The solubility-diffusivity product is unique for each gas/liquid system, and changes exponentially with temperature.

As a result of these investigations, several suggestions have been made concerning design and performance of arterial heat pipes to minimize failures or performance limits attributable to arterial gas occlusions.

Section 1
INTRODUCTION

With the advent of high performance heat pipes utilizing bypass fluid flow avenues for condensate return to the evaporator, the influence of bubbles on the performance of such passages has become an important consideration. The arterial return passage can be a single artery, an artery filled with capillary tubes, a screen covered grooved pipe, an annular passage, or a highly redundant central composite return wick. Of these, the single artery is the configuration most susceptible to the influence of bubbles. It has been suspected for some time that certain types of arterial heat pipe malfunctions are attributable to partial or total blockage of the artery with noncondensible gas. These malfunctions are manifested by very low initial burnout powers at all heat pipe elevations, while heat transport can often be increased to approximately the correct level by allowing the heat pipe to remain idle for several days. This type of behavior is possible with a noncondensible gas occlusion in the artery, because the gas can interfere with capillary pumping, and isothermal conditions allow the gas to diffuse from the artery, eventually collapsing the bubble. In heat pipes with a wall covered by screen or other fine-pore covering, there is a similar potential for gas films to form, increasing ΔT and causing premature burnout.

This program was directed toward generating information which permits a quantitative approach to solving the problem of bubbles. In particular, the underlying philosophy of this program is the amalgamation of experimental data with analytical modeling, each influencing the other, to yield a comprehensive understanding of the mechanisms of bubble generation, transport, and life cycle.

This report discusses venting of arterial bubbles under stagnant conditions. Section 2 presents theoretical aspects of gas bubble dissolution, Section 3 describes experimental apparatus, and Section 4 compares theoretical values with experimental data for physical properties and gas venting times.

It has been shown that the physical properties, solubility and diffusivity, are of primary importance in venting gas occlusions. An apparatus was built to measure these properties for gas/liquid systems from -50° to 100°C. Preliminary investigations indicated significant differences in these properties for various gas/fluid combinations, and the gas/fluid combinations selected for experimentation reflect attendant performance/reliability tradeoffs. Property data obtained were utilized to simulate an arterial heat pipe environment in an apparatus in which an artery is charged with a known amount of gas, and the collapse of the gas occlusion is then observed as a function of time. Venting characteristics generally agreed with theory, and initial estimates of long bubble lifetimes for quite-low impurity levels were confirmed.

Symbols used in this report are as follows.

C	concentration (g-moles/cm^3)
C_a	static gas concentration in sphere, neglecting surface tension (g-moles/cm^3)
C_g	solute concentration in bubble interior (g-moles/cm^3)
C_i	initial concentration of gas solute in solvent (g-moles/cm^3)
C_s	saturation concentration for solute gas in solvent (g-moles/cm^3)
C_γ	concentration attributable to surface tension pressure (g-moles/cm^3)
C_∞	gas concentration in vapor space (g-moles/cm^3)
D	diffusion coefficient (cm^2/sec)
L_o	initial bubble cylindrical length (cm)
P_r	Prandtl number ($C_p\mu/K$)
P_γ	surface tension pressure = $2\gamma/R$ (dynes/cm^2)
P_∞	partial pressure of noncondensible gas in vapor space (dynes/cm^2)
R	interfacial radius (cm)
R_a	fluid tube (artery) radius (cm)
R_e	tube-flow Reynolds number ($\rho DV/\mu$)
R_o	initial bubble radius (cm)
Sc	Schmidt number (ν/D)

T_c	critical temperature
f	fluid saturation fraction (C_i/C_s)
r	radial measure (cm)
t	dissolution time from $R = R_o$ (sec)
t_v	total time to vent a bubble of initial radius R_o (sec)
t*	dimensionless time (Dt/R_o^2)
Δr	arterial wall thickness (cm)
α	Ostwald coefficient, solute concentration in liquid phase/concentration in gaseous phase
γ	surface tension (dynes/cm)
δ	ratio of surface tension pressure to the sum of static pressures
ρ^*	$(C_s - C_i)/C_g$
τ	correction factor to quasi-stationary model vent time
ν	Kinematic viscosity (cm^2/sec)
λ	arterial-wall transmission factor

Section 2

THEORETICAL ANALYSIS OF ARTERIAL BUBBLE DISSOLUTION

The application of experimental data obtained in this program depends on valid modeling of the physical processes occurring within a heat pipe. This section discusses the theoretical aspects of arterial bubble venting, in particular, the interrelationships of diffusion and solubility, and arterial geometry. The idealized situation of a spherical bubble in an infinite media is discussed, followed by an analysis of arterial gas dissolution. The infinite media solution is significant because the experimental method of diffusivity measurement in this program relies on an accurate representation of this collapse phenomena.

2.1 BUBBLE DISSOLUTION IN AN INFINITE MEDIUM

If a spherical bubble of gas, with instantaneous diameter R, is dissolving in an infinite fluid medium, the time-dependent radial concentration field is given by the diffusion equation in spherical coordinates about the center of the gas bubble as

$$\frac{\partial c}{\partial t} + \left(\frac{R}{r}\right)^2 \frac{dR}{dt} \frac{\partial C}{\partial r} = D\nabla^2 C = D\left(\frac{\partial^2 c}{\partial_r 2} + \frac{2}{r}\frac{\partial c}{\partial r}\right) \qquad (1)$$

The velocity term involving dR/dt, not usually included, is necessary to account for the inward-moving fluid as the bubble dissolves, i.e., the necessary inclusion to reflect the moving boundary.

Governing boundary conditions are

$$C(r, o) = C_i \qquad r>R \qquad (2)$$

$$C(r, t) = C_g \qquad r<R \qquad (3)$$

$$C(R, t) = \alpha C_g = C_s \qquad (4)$$

$$R\Big|_{t\,=\,0} = R_o \tag{5}$$

$$\frac{dR}{dt} = \frac{D\ \frac{\partial c}{\partial r}\Big|_{r\,=\,R}}{Cg} \tag{6}$$

Equation 6 implies bubble size change results solely from diffusion at the liquid-gas interface, a basic assumption of this analysis. In addition, the concentration of gas in the vapor phase and gas in the liquid phase is assumed negligible compared to the concentration of solvent in the solvent phase at all times. Generally, the following dimensionless variables are introduced.

$$R^* = \frac{R}{R_o}\ ;\quad r^* = \frac{r}{R_o}\ ;\quad t^* = \frac{Dt}{R_o^2}\ ;\quad \rho^* = \frac{C_s - C_i}{Cg}\ ;\quad C^* = \frac{C - C_i}{C_s - C_i} \tag{7}$$

with these variables, Equation 1 is given as

$$\frac{\partial c^*}{\partial t^*} - \left(\frac{2}{r^*} - \left(\frac{R^*}{r^*}\right)^2 \frac{dR^*}{dt^*}\right) \frac{\partial c^*}{\partial r^*} - \frac{\partial^2 C^*}{\partial r^{*2}} = 0 \tag{8}$$

This governing differential equation appears in similar form in References 1, 2, and 3. The boundary conditions are then

$$C^*(r^*,\ 0) = 0 \qquad r^* > R^* \tag{9}$$

$$C^*(R^*,\ t^*) = 1 \tag{10}$$

$$R^*\Big|_{t^*\,=\,0} = 1 \tag{11}$$

$$\frac{dR^*}{dt^*} = \rho^*\ \frac{\partial c^*}{\partial r^*}\Bigg|_{r^*\,=\,R^*} \tag{12}$$

For the remainder of this discussion, the asterisk symbolism is dropped, and unless specifically noted, the discussion concerns the dimensionless solutions. The boundary conditions, as stated, are for a situation in which the effects of surface tension can be neglected. That is, if surface tension were included, C(R, t) increases as the bubble shrinks, because of the pressure term $2\gamma/R$. Discussion of this situation is deferred to present the general theoretical base.

A closed-form solution to Equation 8 is obtainable only for bubble growth from zero initial size (Reference 1). For bubble dissolution from some initial size R_o, either approximations to Equation 8 must be made, or the

second-order nonlinear equation must be solved by numerical methods. For this program, both approaches have been used. The numerical solution ensures accuracy of experimental diffusivities obtained from bubble dissolution, while useful engineering relationships can be obtained in closed form if certain approximations are made. These short-cut solutions for the most part, are sufficiently accurate to characterize arterial bubble dissolution.

Possibly the most often used approximation to Equation 8 is that in which the mass transport term is neglected. At each point in dissolution, the bubble is assumed to be in equilibrium with the diffusion profile characteristic of a sphere of that size. The quasi-steady state differential equation is

$$\frac{\partial c}{\partial t} - \frac{2}{r}\frac{\partial c}{\partial r} - \frac{\partial^2 c}{\partial_r 2} = 0 \tag{13}$$

By anology with the solution to the heat equation in spherical coordinates (Reference 4), Equation 12 becomes

$$\frac{dR}{dt} = -\rho\left(\frac{1}{R} + \frac{1}{(\pi t)^{1/2}}\right) \tag{14}$$

If the collapse rate is very slow, it has been postulated that the term $1/(\pi t)^{1/2}$ can be disregarded, because it contributes only to the initial dissolution phase. If this term is disregarded, the total dimensionless time for a spherical bubble to disappear (the vent time) in an infinite media is

$$t_v = \frac{1}{2\rho} \tag{15}$$

or in dimensioned variables,

$$t_v = \frac{R_o^2}{2\alpha D(1-f)} \tag{16}$$

where f is the percent saturation of the solution in which the sphere is dissolving. If the term $1/(\pi t)^{1/2}$ is included, the complete solution to Equation 14 is

$$t_v\left(1+2\sqrt{\frac{1}{\pi t_v}}\right) = \frac{1}{2\rho} \tag{17}$$

In a numerical solution of the exact differential Equation 8, Duda and Vrentas (Reference 6) presented a correction factor to the vent time as given by Equation 15, so that

$$t_v = \frac{\tau}{2\rho} \tag{18}$$

The correction factor is shown in Figure 2-1 as a function of ρ. Also presented is the correction factor τ', when Equation 17 is considered exact. This expression, in fact, underestimates true vent time. Inclusion of the moving boundary impedes dissolution on this basis.

For diffusivity measurements, it is critical that the exact radial time profile be known, and a computer code was developed to solve Equation 8 by an implicit method in which systems of linear algebraic equations are solved by Gaussian elimination. A detailed discussion of the technique is presented in Reference 7. For $\rho \leq 1$, $\sim$ 400 time steps were generally adequate to describe the dissolution phenomena, along with 150 dimensionless radial steps in ψ-space, as discussed in Reference 6. Figure 2-2 shows a comparison between tabulated numerical results from Reference 6 and results from this study. The comparison is very good. Also included are Equation 15 and 18 for comparison. Equation 15 is a poor approximation to the exact solution; Equation 18 is correct on vent time, but errs on the radial time-dependent profile. Both equations become better approximations as ρ goes to zero, as indicated in Figure 2-1. In the following analysis, although the model is possibly too simple, the method used in developing Equation 15 is used for three reasons. First, the gas/liquid systems under consideration generally have small ρ, making the approximations more reasonable; second, knowing the venting times to within a factor of two is generally adequate, and third, the equations resulting allow inspection of closed-form expressions which are useful in understanding tradeoffs between performance and reliability.

2.2 BUBBLE DISSOLUTION WITH SURFACE TENSION

Analysis of bubble dissolution in surface-tension-dominated systems has been reported in the literature to a much lesser extent than has the case of a constant interfacial concentration. Equation 8, which governs, is still valid, but the boundary conditions must be stated differently. A new dimensionless parameter, δ, expresses the size of surface tension pressure relative to the summed static pressures on the sphere, as

$$\delta = \frac{2\gamma/Ro}{P_a} = \frac{C_\gamma}{C_a} \qquad (19)$$

2593

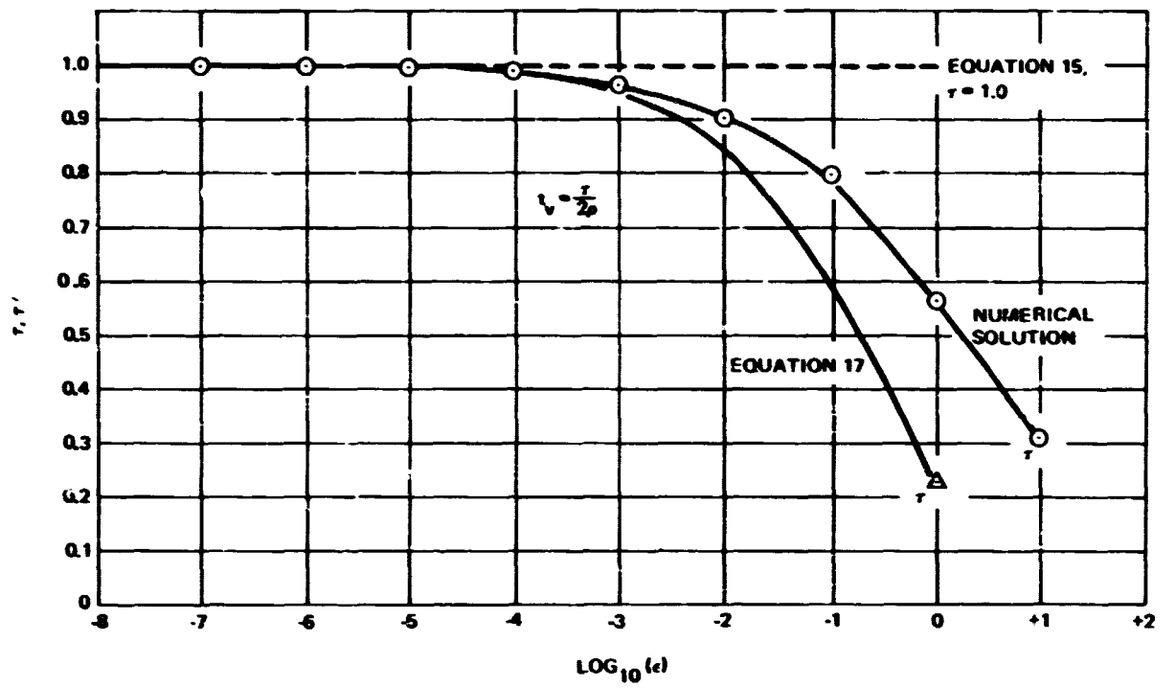

Figure 2-1. Correction Factor for Vent Time

2594

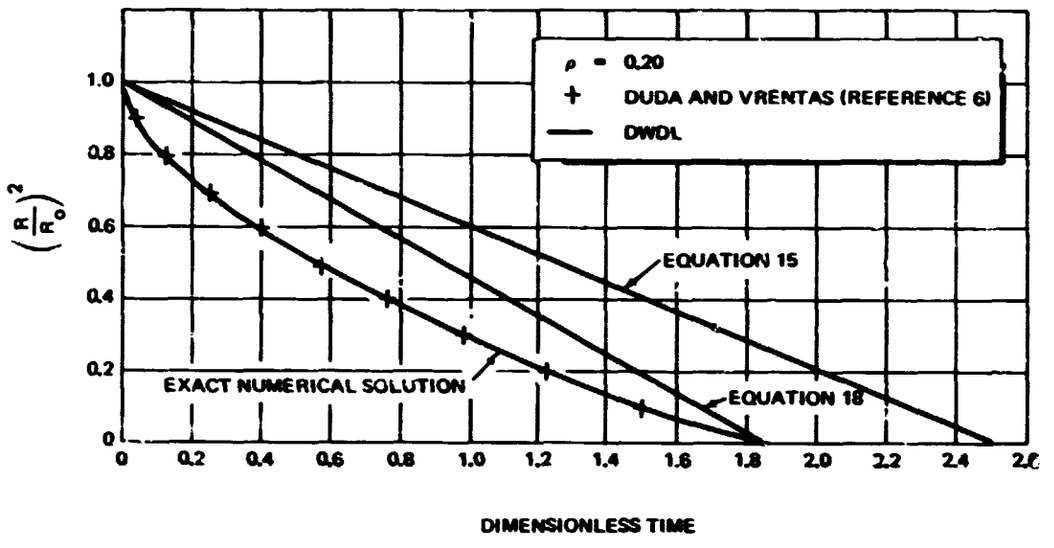

Figure 2-2. Comparison of Time-Dependent Radius Calculations for a Dissolving Sphere

P_a is that pressure at the bubble position if the bubble radius of curvature were infinite. The sum P_a includes, for example, gravity head, ρ_{pgh}, either positive or negative, ΔP_{SAT}, the vapor pressure differential between the bubble site and the general fluid surface, and P_∞, the partial pressure of gas above the liquid phase. All are assumed constant in value. The boundary conditions 9, 10, 11, and 12 are then

$$C(r,0) = 0 \qquad r>R \tag{20}$$

$$C(R,t) = \left[(1 + \delta/R)/(1+\delta) - f\right]/(1-f) \tag{21}$$

$$R\Big|_{t=0} = 1 \tag{22}$$

$$\frac{dR}{dt} = \frac{\rho}{1 + 2/3\,\delta/R} \cdot \left.\frac{\partial c}{\partial r}\right|_{r=R}; \qquad \rho = \frac{C_s - C_i}{C_a} \tag{23}$$

$$C_s = \alpha C_g(1, 0) \tag{24}$$

Again, the total differential equation cannot be solved formally with condition (23). If, as in Section 2.1, the convective term is disregarded, the quasi-steady-state differential equation for collapse rate replacing Equation 14 is

$$\frac{dR}{dt} = -\frac{\alpha(GR + \delta)}{(R + 2/3\,\delta)}\left(\frac{1}{R} + \frac{1}{(\pi t)^{1/2}}\right) \tag{25}$$

where $G = 1 - C_i/\alpha C_a$

Equation 25 is formally integrable if the term $1/(\pi t)^{1/2}$ is disregarded. With this modification, which parallels the process of Section 2.1, dimensionless vent time is

$$t_v = \frac{1}{\alpha S^2}\left[\frac{2}{3}\left(S - \ln(1+S)\right) - \frac{1}{G}\left(S - \frac{S^2}{2} - \ln(1+S)\right)\right] \tag{26}$$

where $S = G/\delta$

Two cases are of particular importance. In the limit of a completely surface-tension dominated bubble where $\delta \to \infty$, the dimensionless vent time is

$$t_v = \frac{1}{3\alpha} \tag{27}$$

and for diffusion into a saturated solution, where $G \to 0$,

$$t_v = \frac{1}{3\alpha} \cdot \left(1 + \frac{1}{\delta}\right) \tag{28}$$

These equations are closed-form estimates for non-isothermal, but stagnant, dissolution collapse of a spherical bubble into an infinite body of fluid. Allowance has been made for surface tension, partial pressure of noncondensible gas in the vapor space, gravity head, etc.

2.3 APPLICABILITY OF INFINITE MEDIA SOLUTIONS

In general terms, the infinite media solutions for vent time are most applicable if the bubble radius is less than 1/10 the smallest characteristic radial dimension of the enclosure in which it is contained. For example, if the bubble is in an R_a radius artery, then the maximum bubble radius is approximately 0.1 R_a. This "rule-of-thumb" results from numerical analysis of the concentration field about a bubble, which showed that most of the non-zero concentration field is within 5 to 10 radii of the surface. Figures 2-3 and 2-4 show the locus of several concentrations as a function of time for = 0.01 and 1.0. The profile $c^* = 1$ is at the bubble interface, and therefore also shows the bubble radius as a function of time. As far as solute penetration is concerned, most of the initial bubble mass is distributed within 5 to 10 radii of the bubble for the * range chosen. This range is typical of an impurity gas bubble venting, but is not typical of venting in an isothermal gas-controlled heat pipe where * can be very small. Under flow conditions, the small diffusive penetration means that most of the significant solute is removed within a few radii of the bubble, thereby relieving some of the restrictions to modeling the dissolution of a spherical particle in a cylindrical tube, because only flow in the immediate vicinity of the bubble must be considered.

Liebermann, (Reference 8) reports that a spherical bubble contacting a flat surface requires $1/\ln 2$ longer time to collapse because of the buildup of solute at the surface, in analogy with a problem in electrostatics. This factor must also be considered, as well as the fact that a bubble residing against a thin fluid film, as might be contained in an artery wall, may vent more rapidly. However, for purposes of an engineering model, the effects of walls on the static venting of spherical bubbles is a correction beyond the scope of this program, and is generally neglected. That is, a spherical bubble with a diameter equal to or less than R_a, is assumed to vent in the time given by Equation 26. The validity of this assumption is discussed in Section 4.2, which compares theoretical and experimental collapse of arterial occlusions.

2595

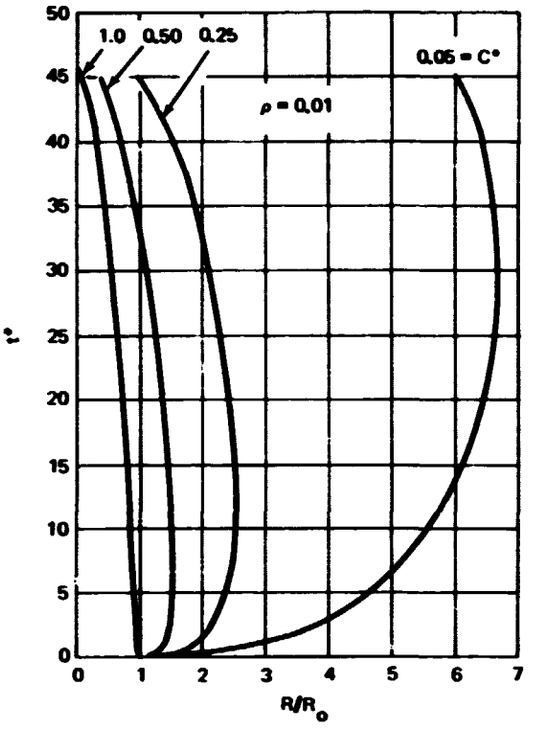

Figure 2-3. Concentration Profiles of a Dissolving Sphere

2596

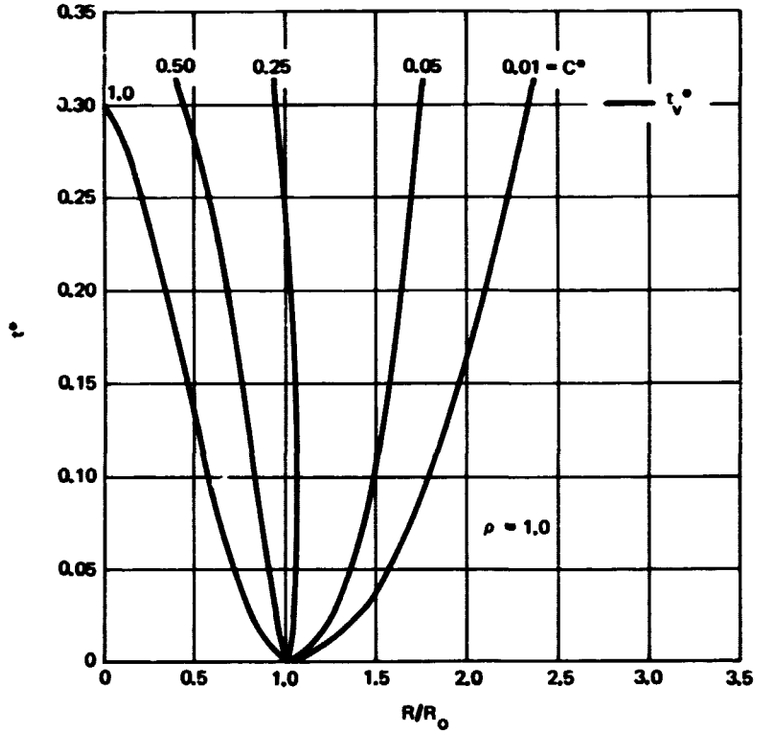

Figure 2-4. Concentration Profiles of a Dissolving Sphere

Several important conclusions can be drawn from these engineering models. When the dimensionless time variable is solved for the real vent time, the vent time is in general given by

$$t_v = \frac{R_o^2 \, g(f)}{N \alpha D} \tag{29}$$

where N varies from 2 to 3 and g(F) is a function relating the dissolution time to the initial solute concentration in the solvent. The importance of the property grouping αD is apparent. As will be shown in Section 4.1, the experimental solubility-diffusivity product is considerably different for each gas/liquid combination, and is exponentially dependent on temperature. Figure 2-5 shows early theoretical estimates of the factor $1/\alpha D$, designated the venting parameter. Considerable variability in venting parameter is apparent.

Venting time is also proportional to the square of the initial bubble radius. This implies that considerably more stability against arterial occlusion is possible, if the artery is decreased in size. This, however, is possible only at a loss in artery performance.

A factor not yet discussed is the function g(F). For the condition in which static gas pressure of the system is much less than the surface tension pressure $2\gamma/R_o$, the function g(F) is unity, that is, there is little effect of percent saturation of fluid on venting, and the real vent time is

$$t_v = \frac{R_o^2}{3 \alpha D} \tag{30}$$

This condition can occur when the gas source is a trace impurity of the system, or $P_\infty << 2\gamma/R_o$, and gravity head and vapor pressure differentials are negligible. For an isothermal arterial dump which initially removed fluid from a section of artery L_o in length and compresses it to a bubble of diameter R_o, vent time is given approximately by Equation 30, with R_o^2, given by

$$R_o^2 = \left(\frac{3}{8}\right)\left(\frac{P_\infty R_a^2 L_o}{\gamma}\right) \qquad R_o \leq R_a \tag{31}$$

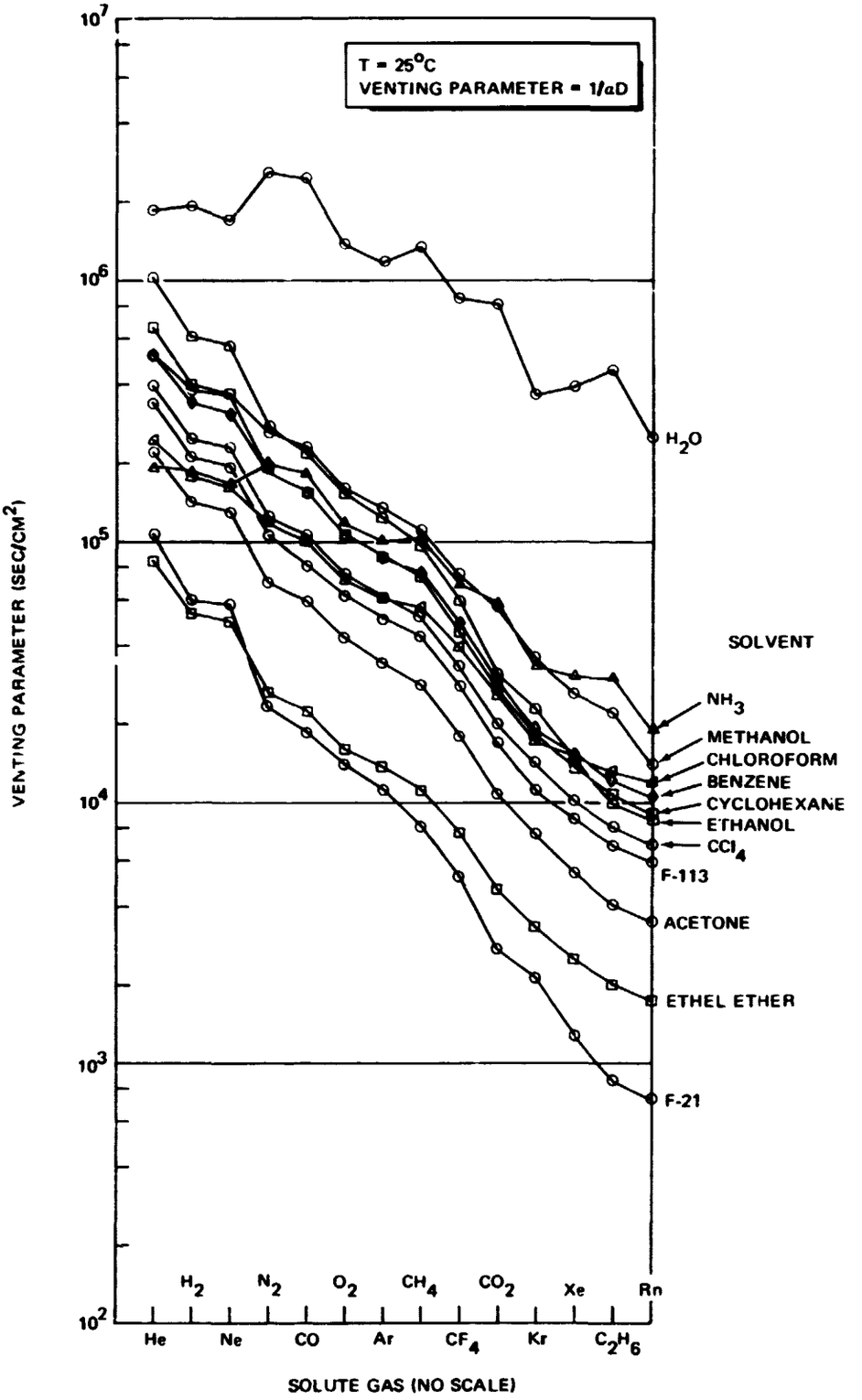

Figure 2-5. Venting Parameter for Various Gas/Liquid Combinations

Equations 30 and 31 relate bubble vent time when there is a small impurity gas level P_∞, an artery of radius R_a, and a gas-fluid property group ($\sigma \alpha D$). If L_o is established equal to the total artery length, then t_v is the maximum time under isothermal conditions that the artery could be inoperative attributable to a trace-gas bubble. Table 2-1 presents representative trace-gas venting times for the fluids investigated, as well as water.

When noncondensible gas (NCG) pressure and other pressure differentials are significant compared to $2\ \gamma/R_o$, Equation 30 is not applicable. In general, if a heat pipe has been in an isothermal condition for about one hour, NCG in the liquid and vapor phases is in equilibrium and the solution is saturated. The governing equation for bubble vent time is then Equation 28. In terms of dimensioned variables,

$$t_v = \left(\frac{R_o^2}{3\alpha D}\right)\left(1 + \frac{P_a}{2\gamma/R_o}\right) \tag{32}$$

Table 2-1

VENTING OF A TRACE IMPURITY GAS BUBBLE

Fluid	Temperature (°C)	t_v (sec) helium	t_v (sec) argon
Ammonia	-40	1200	107
	20	63	6.7
	60	7.0	1.6
Freon-21 ($CHCl_2F$)	-40	367	43
	20	67	17.5
	60	23	7.5
Methanol	-40	1030	154
	20	133	55
	60	50	26
Water	22	1481	1215

$t_v = R_o^2/3\alpha D$ $\qquad$ $R_o = 0.050$ cm

This solution is significant. Vent time increases linearly with NCG pressure with other factors constant. In addition, pressure $2\gamma/R_o$ is on the order of 0.01 psia for organic fluids and a typical 0.05-cm radius bubble; a rather small P_a can then significantly increase dissolution time. Physically, gas concentration within the bubble increases linearly with NCG pressure, but the diffusion gradient into the saturated solution remains constant because it is only determined by the excess pressure attributable to the surface tension effect. The net result is a vent time increase proportional to NCG pressure.

Substituting actual values for helium and ammonia into Equation 31, $1/\alpha D \sim 75,000$ cm^2/sec at 20°C (Section 4.1). If $R_o = 0.05$ cm and $P_a << 2\delta/r_o$, then $t_v = 1.0$ minutes. If $P_a = 1.0$ mm Hg, then $t_v = 2.8$ minutes. This corresponds to a helium impurity level of only 130 ppm in the vapor. If, as in a gas-controlled heat pipe, the isothermal helium pressure is about equal to the vapor pressure of the ammonia working fluid, then $t_v = 9.0$ days. This is an extremely long time relative to the expected transients associated with controllable heat pipe operation. It is possible to decrease this time by decreasing the maximum bubble size R_o, choosing a different control gas, or using a working fluid with lower vapor pressure. The time required for venting such gas bubbles is in agreement with experimental data presented in Section 4.2.

2.4 DISSOLUTION OF AN ELONGATED BUBBLE

From observations in glass systems, if a bubble is present in an artery, it is statistically more likely to be elongated than any other shape. Therefore, the venting of elongated arterial bubbles is of considerable importance. Analysis of gas loss from an elongated bubble constricted within a tubular artery as in Figure 2-6 has resulted in the following simplified differential equation in real variables.

$$\frac{d\ell}{dt} = 2\alpha D'(1-f)\left[\frac{\ell}{R_a^2 \ln\left(1+\frac{\Delta r}{R_a}\right)} + \frac{2\beta}{\lambda R_a}\right] \qquad (33)$$

where

ℓ = bubble instantaneous length

$D' = \lambda D$

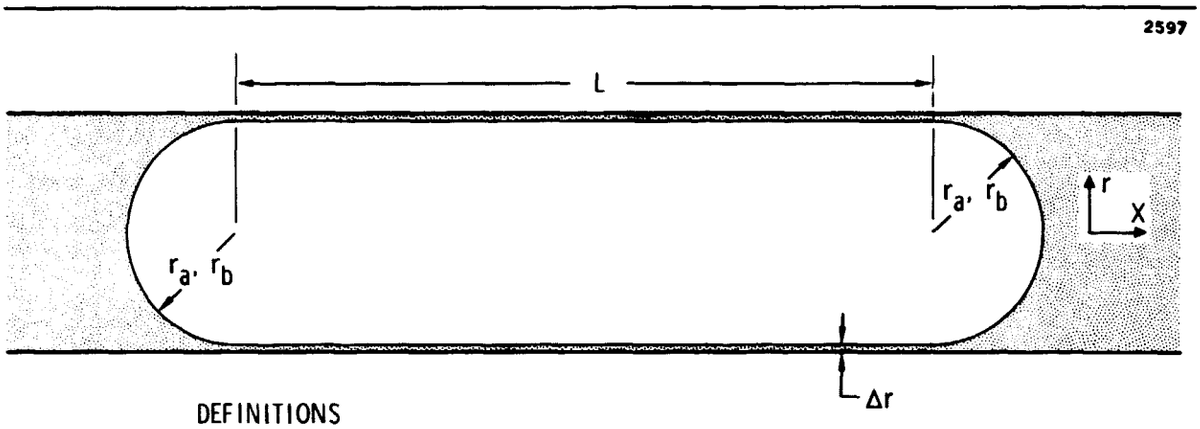

DEFINITIONS

L = INITIAL LENGTH OF BUBBLE CYLINDRICAL SECTION

r_a = ARTERIAL RADIUS = r_b = RADIUS OF HEMISPHERICAL END-CAP

Δr = FLUID FILM THICKNESS OVER CYLINDRICAL SECTION

ASSUMPTIONS
- QUASI-STEADY-STATE (INERTIAL TERMS NEGLECTED)
- ISOTHERMAL CONDITIONS
- HEMISPHERICAL END CAPS
- DIFFUSION-DOMINATED COLLAPSE

Figure 2-6. Arterial Bubble Modeling

λ = wall tortuosity factor

$f = C_\infty / C_g$

Δr = arterial wall thickness

β = end-cap diffusion factor (~ 1)

The derivation of Equation 33 is included in Appendix B. The total time for a bubble of length ℓ_o to vent down to a spherical shape is

$$t_1 = \frac{R_a^2 \ln\left(1 + \frac{\Delta r}{R_a}\right)}{2\alpha D'(1-f)} \ln\left(1 + \frac{\lambda \ell_o}{2\beta R_a \ln\left(1 + \frac{\Delta r}{R_a}\right)}\right) \quad (34)$$

The property grouping αD is again important to venting, as is the factor (1-f). Because of the complex diffusion path through the screen fluid layer, the factor λ is included to form an effective diffusion coefficient D'. The factor λ changes as the composition of the artery wall is altered by screen size change, etc.

To minimize gas vent time, it is desirable to decrease R_a, Δr, ℓ_o, and f, and increase αD. If the bubble is quite elongated, the length of the bubble decreases by a factor of two, independent of initial size, in the period

$$\tau_{1/2} = \frac{0.693\ R_a^2\ \ln\ (1+\frac{\Delta r}{R_a})}{2\alpha D'\ (1-f)} \qquad (35)$$

Table 2-2 gives half-lives for a representative arterial gas-controlled design for various gas/liquid combinations at 20°C. It is assumed that control gas pressure is equal to vapor pressure of the working fluid, and that the artery has been emptied in an isothermal condition. This is a very credible situation. If a pipe is loaded and sealed, then handled such that the elevation is much more than 1 foot from end-to-end at any time, the artery will probably be emptied. Other design criteria appear in Table 2-1.

Bubble half-lives are generally very long, and therefore, the gas affects performance, if testing is done any time before t_1 (as given by Equation 34) has elapsed. The arterial venting tests described in Section 4.2 confirm the time necessary for such arterial bubbles to collapse.

Table 2-2

HALF-LIVES FOR ELONGATED ARTERIAL BUBBLES IN A GAS-CONTROLLED HEAT PIPE AT 20°C

Fluid	$t_{1/2}$ (helium)	$t_{1/2}$ (argon)
Ammonia	7.0 days	17. hr
Freon-21 ($CHCl_2F$)	36. hr	9.5 hr
Methanol	4.8 hr	1.7 hr
Water	3.0 hr	2.5 hr

R_a = 0.050 cm λ = 0.40 Δr = 0.020 cm

Position-independent gas mixture

Artery stem height = 0.0 cm

Noncondensible gas partial pressure equals vapor pressure

2.5 DISSOLUTION OF AN ARTERIAL BUBBLE IN FLOW

It is possible to obtain a closed-form approximation to dissolution of a small bubble associated with low arterial flow. The technique, in essence, assumes that the configuration of a small bubble against an artery wall is very close to the flow geometry of a bubble touching a semi-infinite plane with a parabolic velocity profile parallel to the surface. The approach is discussed in more detail in Appendix C. The vent time for a small bubble in flow is given by

$$t_v \cong \frac{-1}{\alpha} \int_1^0 \frac{R(R+2/3\ \delta)\ dr}{(1+BR)(\delta+GR)}, \qquad R_o \leq 1/2\ R_a \tag{36}$$

where B is a flow parameter given by

$$B = 0.622\left(\frac{R_o}{R_a}\right)\sqrt{Re}\ (Sc)^{1/3} \tag{37}$$

and the Reynolds number is the tube-flow value for the artery containing the bubble.

As an example of the effect of fluid flow on bubble vent time, consider a condition where $\delta >> GR$, that is, surface tension dominates over static pressure. Equation 36 gives the dimensioned vent time as

$$t_v = \frac{2\ R_o^2}{3\alpha DB}\left(1 - \frac{1}{B}\ \ln\ (1+B)\right) \tag{38}$$

Vent time under these conditions is approximately inversely proportional to the factor B and has the familiar dependences on other properties.

To obtain a representative value for B, let $R_o/R_a = 0.25$, Re = 5, and the Schmidt number = 100 ($\mu/$ = 0.01 cm^2/sec, D = 10^{-4} cm^2/sec). The factor B then equals 1.61, and the decrease in bubble lifetime attributable to flow is about 50%, when Equation 38 is compared to Equation 27. Therefore, low flow can significantly decrease the time necessary to dissolve a small gas inclusion, although the arterial pressure drop must also be considered, so that the gas internal to the bubble is at a pressure where dissolution is possible.

2.6 SUMMARY

Various models have been developed for the diverse conditions encountered when gas in entrapped within an artery. All calculations assume the existence of an arterial gas occlusion. The various means by which such a gas plug can be created are diverse, some of the most obvious being excessive elevation of the evaporator section of the pipe, burn-out of the evaporator, and shock effects such as occur at vehicle life-off or payload separation.

The critical factors determining venting time for spherical arterial bubbles are summarized by

$$t_v \cong \frac{R_o^2 \, g(f)}{N \alpha D}$$

where R_o is the initial bubble radius, αD is the solubility-diffusivity product, N is a constant $\sim$2-3, and g(f) is the forcing function which signals either dissolution or growth, depending on gas concentration inside the bubble and in the outside fluid. Table 2-1 summarizes venting times for surface-tension-dominated dissolution of a trace gas impurity.

Dissolution of an elongated bubble is characterized by a half-life, i.e., the time needed to collapse the bubble to 1/2 its original size (Equation 35). Various half-lives are given in Table 2-2. The factors discussed for spherical bubbles are of importance in the venting of elongated bubbles and, in addition, vent time depends on arterial wall thickness.

Low flow in the artery can significantly assist dissolution and shorten bubble lifetime, and a flow parameter quantifying this assistance is identified (Equation 37).

Possibly the most critical finding of this analysis is the extremely long times necessary to vent gas occlusions when these occur in gas-controlled heat pipes. This results from the large quantity of gas in any one bubble, and the insignificant surface tension driving force causing dissolution. Experimental data presented in Section 4.2 confirm the long calculated vent times.

Section 3

EXPERIMENTAL APPARATUS

The experimental phase of this program was oriented towards collecting property data and using that data in an arterial simulator to produce valid working models of gas dissolution from within heat pipe arteries. To achieve that goal, an apparatus was constructed to measure the solubility and diffusivity of gases in liquids over a wide temperature range, and arterial simulators were constructed to observe the venting of gas occlusions from screened arteries under static conditions.

3.1 SOLUBILITY-DIFFUSIVITY APPARATUS

An apparatus has been constructed to measure both solubility and diffusivity of gases in liquids. Construction materials are principally Type 304 and 316 stainless steel, with a limited number of Teflon seals. All materials are generally compatible with methanol, Freon-21, and ammonia, the fluids used in this program. Thermal and pressure-limits on this apparatus are shown in Table 3-1, along with other pertinent physical characteristics.

Solubility is measured in terms of the Ostwald coefficient. The Ostwald coefficient of a gas in a liquid is experimentally determined by the isothermal mixing of a known amount of gas and a known amount of liquid in a fixed two-phase volume. After some time and agitation, the liquid becomes gas-saturated and an equilibrium between the molar concentration of gas in the liquid and vapor phases is attained. Basic arrangement of the apparatus is shown in Figure 3-1. A test-fluid pressure vessel of about 500 cc is arranged within a large isothermal vapor chamber. External to the fluid chamber, a coil of tubing with carefully measured volume is pressurized to about 40 psia with the test noncondensible gas. Fluid is introduced to the chamber and the low-pressure side of the pressure differential transducer. The low-pressure side is valved off, then fluid and the complete gas charge are allowed to fill the remainder of the pressure chamber such that the gas-vapor/liquid interface is at the top of the reference reticule. The reticule serves to establish the fluid charge and the new gas

Table 3-1

SOLUBILITY/DIFFUSION APPARATUS THERMOPHYSICAL CHARACTERISTICS

Characteristic	Limitation
Materials compatibility	Type 304 and 316 stainless-steel construction. Two Teflon seals. Stainless-steel bellows valves. Cast-iron observation port piece.
Operating temperature range	-100° to 121°C. Low temperature limited at present to -50°C by Buna-N seals stiffening and cracking. High temperature limited by warranty specifications on pressure transducer.
Operating pressure range	0 to 300 psig. Magnetically coupled pump rated at 300 psig. Pressure transducer rated at 1000 psig line pressure. Observation port window rated at 1000 psig.
Transducers	Copper-constantan and chromel-alumel thermocouples. Pressure transducer is Validyne variable reluctance 0 to 50 psid range device. Transducer is stainless steel on both high and low pressure sides; temperature range is -100° to 121°C.
Pump loop	Pumped by variable-speed, magnetically-coupled centrifugal pump. At maximum flow, test chamber fluid is changed twice per minute. 300 psig pressure rating; -54° to 121°C temperature range.
Pressure vessel	Parr Instrument Co. Model 4762. 3000 psig; 350°C, Teflon gasket. 472 cc volume. Type 316 stainless-steel body.
Bubble generator	0.01 cm orifice, 0.1 dia bubbles via two-stage sorter. Bubbles produced by charging orifice volume from controlled gas source.

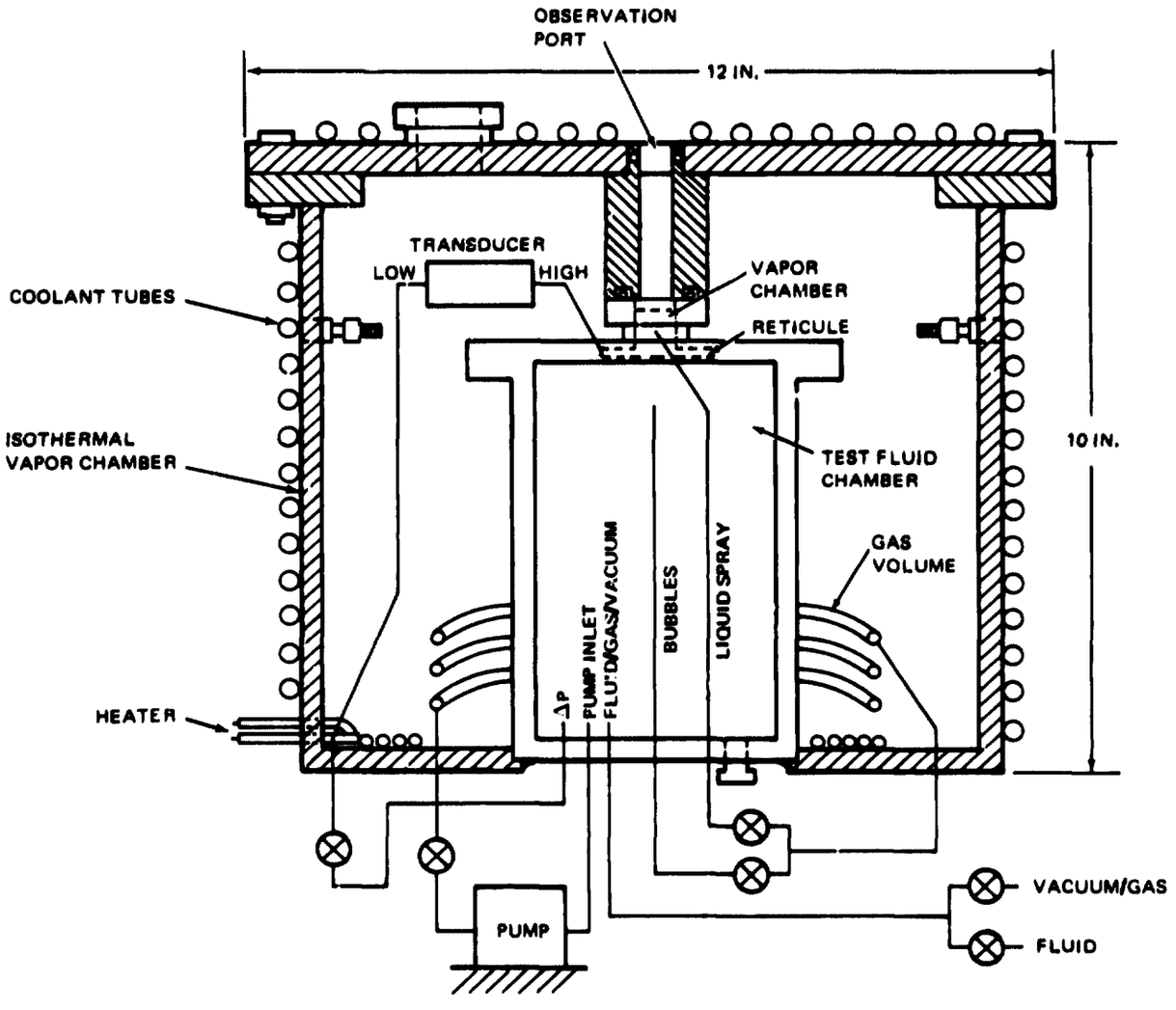

Figure 3-1. Solubility/Diffusion Apparatus General Arrangement

charge density in the vapor chamber above the reticule. The magnetically coupled stainless-steel pump is energized so that fluid is sprayed through the vapor chamber, into the fluid pool, down to the bottom, and through the cycle as many times as necessary to establish an equilibrium concentration of dissolved gas in the liquid. Progress is monitored with the pressure differential transducer as a gradual drop in vapor chamber pressure. When the reaction has proceeded to equilibrium, pressure differential is noted. Because the reference side is pure clean fluid at the same temperature, then the pressure differential must result solely from noncondensible gas remaining in the vapor chamber. Knowing the vapor chamber volume, fluid volume, and initial gas charge in moles, the amount of gas lost to the liquid, and therefore, solubility can be calculated. This process is repeated at each temperature of interest.

The diffusion coefficient is found by the disappearing bubble technique. Prior to the solubility studies, small gas bubbles are injected to the underside of the reticule. The gradual dissolution of these spherical bubbles in the gas-free fluid is related to both solubility and gas/liquid diffusivity. Elimination of solubility from the expressions is possible because of experimental solubility values established in the solubility-phase of the experiment. Because of the necessity for an accurate model to relate measurements, the governing differential equations are solved by numerical methods. The technique is relatively new, one of the first attempts at using the method described in Reference 8 in 1957. It was not until 1969 that a satisfactory numerical analysis method for the complete second-order equation was documented in the literature (Reference 3).

The technique affords a simple, fast means of diffusivity determination, and is usable over a broad temperature range. Its limitations are mainly sensitivity to vibration and diffusion cell convection currents which disturb the concentation field about the bubble. At higher temperatures, another problem occurs, in that, dissolution is so rapid (~10 sec) that the effects of placing the bubble in position may significantly affect dissolution rates. The method, in general, works best when the vent time for the bubble is long (greater than about 100 seconds), and fluid viscosity is high.

The diffusivity is obtained by a cross-plot of collapse profile such as Figure 2-2 against the experimental collapse profile. The common axis used is $(R/R_o)^2$, so that a plot of real time versus dimensionless time should yield a straight line of slope β, and the diffusivity is equal to $R_o^2/(0.693\beta)$. The factor 0.693 is included to allow for the contacting plane against which the bubble rests. Figure 3-2 presents an experimental cross-plot; Figure 3-3 shows a view through the apparatus observation port.

3.2 ARTERIAL SIMULATION APPARATUS

The property data obtained with the solubility-diffusion apparatus were used to calculate venting times for bubbles within a screened artery such as in the isothermal fluid/vapor heat pipe apparatus shown in Figure 3-4. This device, used to observe bubble collapse under more realistic conditions, is in essence a nonthermally pumped simulated heat pipe and artery. An injection block introduces gas bubbles into the artery. A sight port is used to monitor the size of the bubble produced. Once a bubble of proper size has been created, flow is increased to move the bubble into the glass observation section, then adjusted to an experimental flow, or no flow. A nickel wire in the injection block can be heated to form a vapor bubble. This vapor bubble can then be observed in the same manner as a noncondensible bubble. The glass Dewar-type observation area is about 5 in. long; the entire isothermal environment is approximately 12 in. long. Chamber temperature is regulated by a heater/cooler in conjunction with a circumferential heat pipe; this heat pipe completely surrounds the metal section of the chamber.

Various thermophysical characteristics of this apparatus are given in Table 3-2. Perhaps the most important is the limitation of internal pressure to 30 psia because of the glass envelope. This limits fluid selection somewhat, as well as temperature range, because high-pressure working fluids such as ammonia cannot be used.

2598

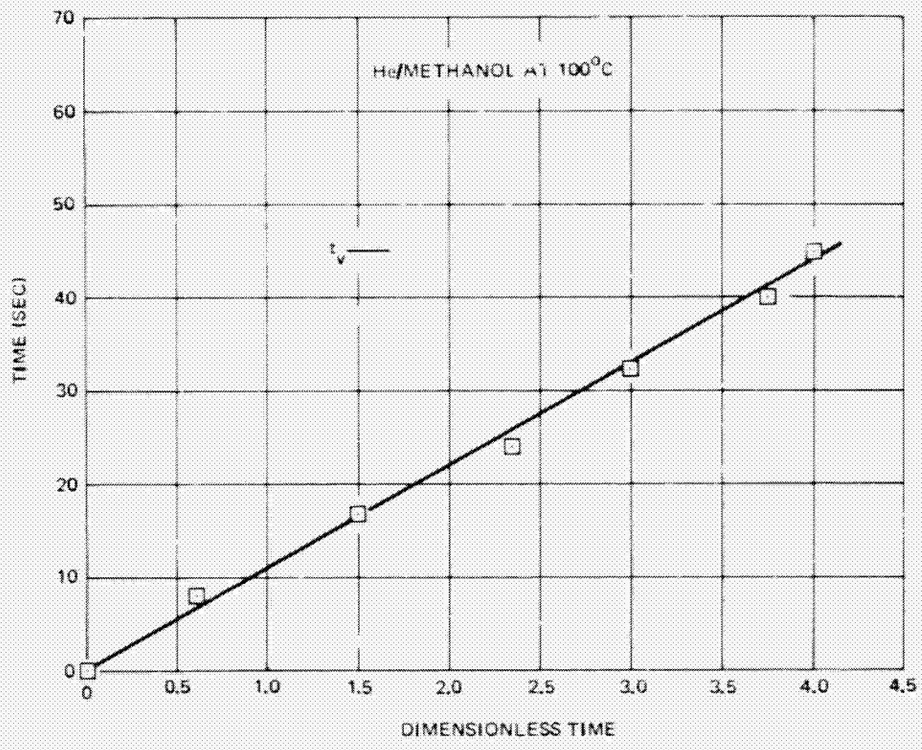

Figure 3-2. Cross-Plot of Theoretical and Experimental Bubble Collapse

2599

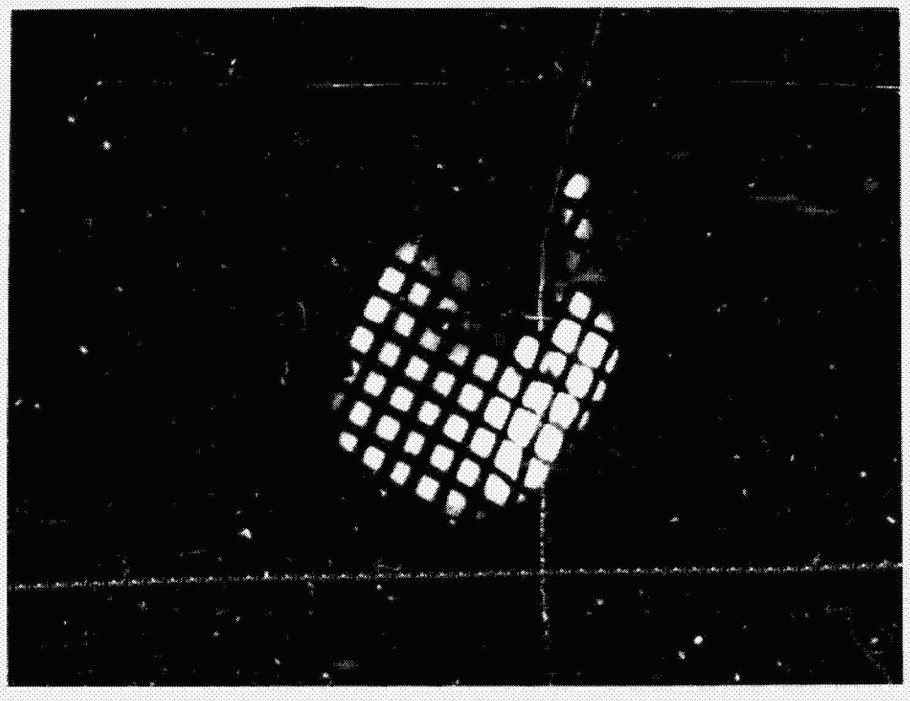

Figure 3-3. Apparatus Observation Port

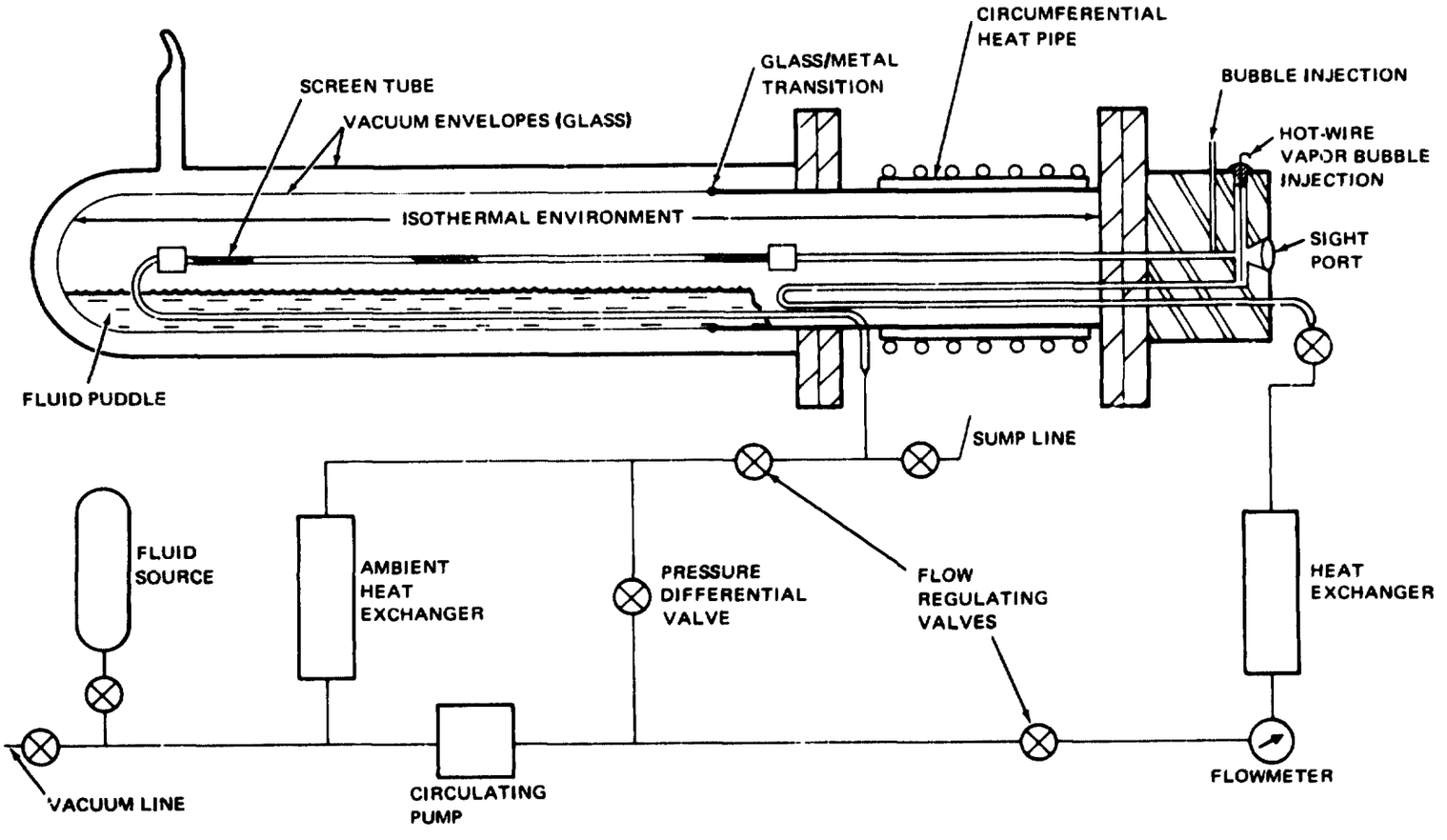

Figure 3-4. Arterial Simulation Apparatus General Arrangement

Table 3-2

PUMPED ARTERY THERMOPHYSICAL CHARACTERISTICS

Characteristic	Limitation
Materials compatibility	Borosilicate glass viewing area. Type 304 stainless steel, Kovar, nickel, and nickel-based braze metals in contact with fluid and vapor. Some Nylon, Teflon, and Buna-N seals. Stainless steel bellows valves, and copper flange gaskets.
Operating temperature range	-50° to 200°C. Low temperature limited by expansion of Teflon seals. High temperature limited by melting of solder.
Operating pressure range	0 to 15 psig. Glass observation envelope stress limitation.
Transducers	Copper-constantan and chromel-alumel thermocouples.
Pump loop	Pumped by variable speed double-acting bellows. 15 psig pressure rating.
Flowmeters	3 Tri-Flat calibrated glass flowmeters in a parallel switched array. Total range of array is 0.059 to 107 cc/min of water. Other fluids will have a similar range of flow.
Bubble injection	0.01 cm orifice and needle valve. Heated nickel wire in injection block for production of vapor bubbles.

Section 4
EXPERIMENTAL RESULTS

The discussion of experimental data is divided into two parts. The first considers measurements of the solubility and diffusivity of helium and argon in ammonia, Freon-21 ($CHCl_2F$), and methanol. The second discusses experimental data taken of gas occlusions venting from screened arterial passages with Freon-21 and methanol.

All fluids used for the measurements of physical property data and venting effects were distilled to a total noncondensible partial pressure of less than or equal to 10^{-2} atmosphere, or purchased with the required certified purity. Ammonia was purchased certified to have less than 150 ppm noncondensible gas and less than 20 ppm water impurity levels; the methanol was Baker certified spectrophotometric quality; the Freon-21 was purchased from E. I. Dupont De Nemours & Co., Inc. Helium and argon gases were 0.9999 pure.

4.1 PHYSICAL PROPERTY DATA

The solubility of argon and helium in ammonia, Freon-21, and methanol is presented in Figures 4-1, 4-2, and 4-3, and Table 4-1. Figure 4-4 presents solubility of a number of gases in water as compiled by Himmelbau, (Reference 16). The behaviorisms of the gas/fluid combinations of this investigation are similar to the same species or like diameter species in water. In general, the molecules with smallest diameter are influenced the most by temperature. Minima in solubility, exhibited by gases in water, are not present over the investigated temperature range, or are of smaller size in the fluids investigated in this program. For example, argon in methanol may exhibit a minima in solubility versus temperature, although accuracy of the data may not warrant such a conclusion. Experimental uncertainty for all gas/liquid combinations is shown in Table 4-1. All partial pressures of noncondensible gas at equilibrium ranged from 10 to 50 psia, and therefore, it is not expected that deviations from Henry's law were encountered. Solubility theory is discussed in detail in Appendix A.

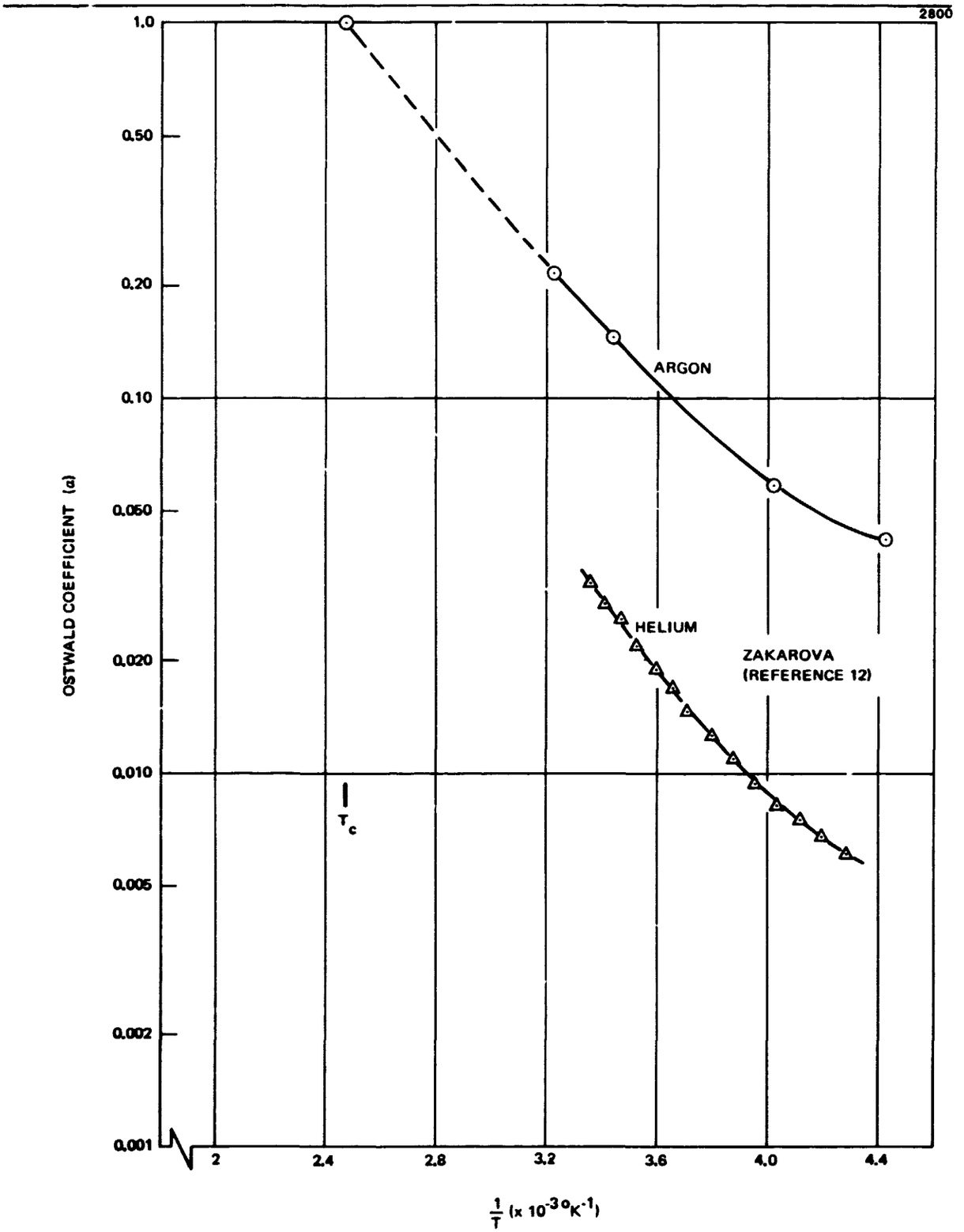

Figure 4-1. Solubility of Helium and Argon in Ammonia

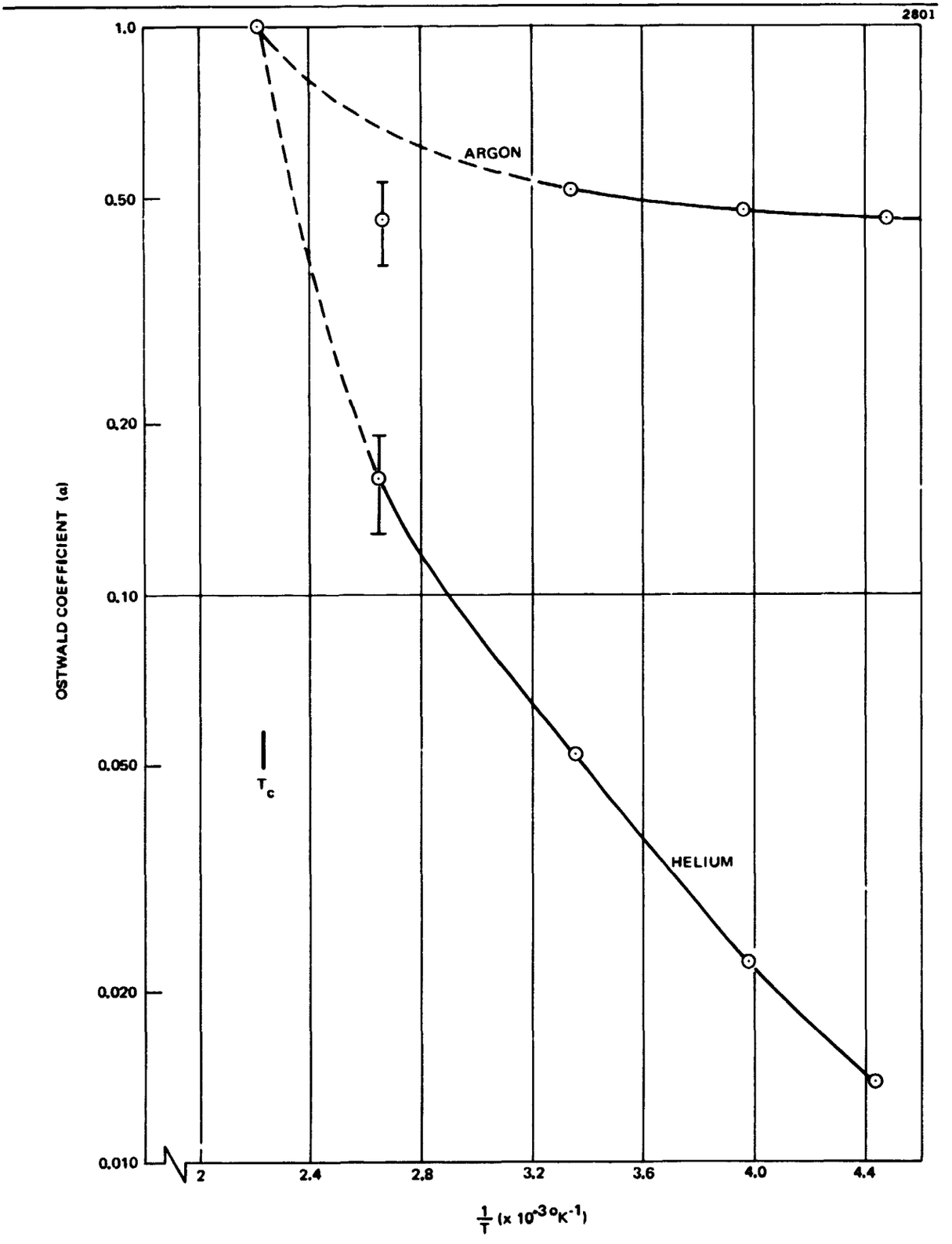

Figure 4-2. Solubility of Helium and Argon in Freon-21

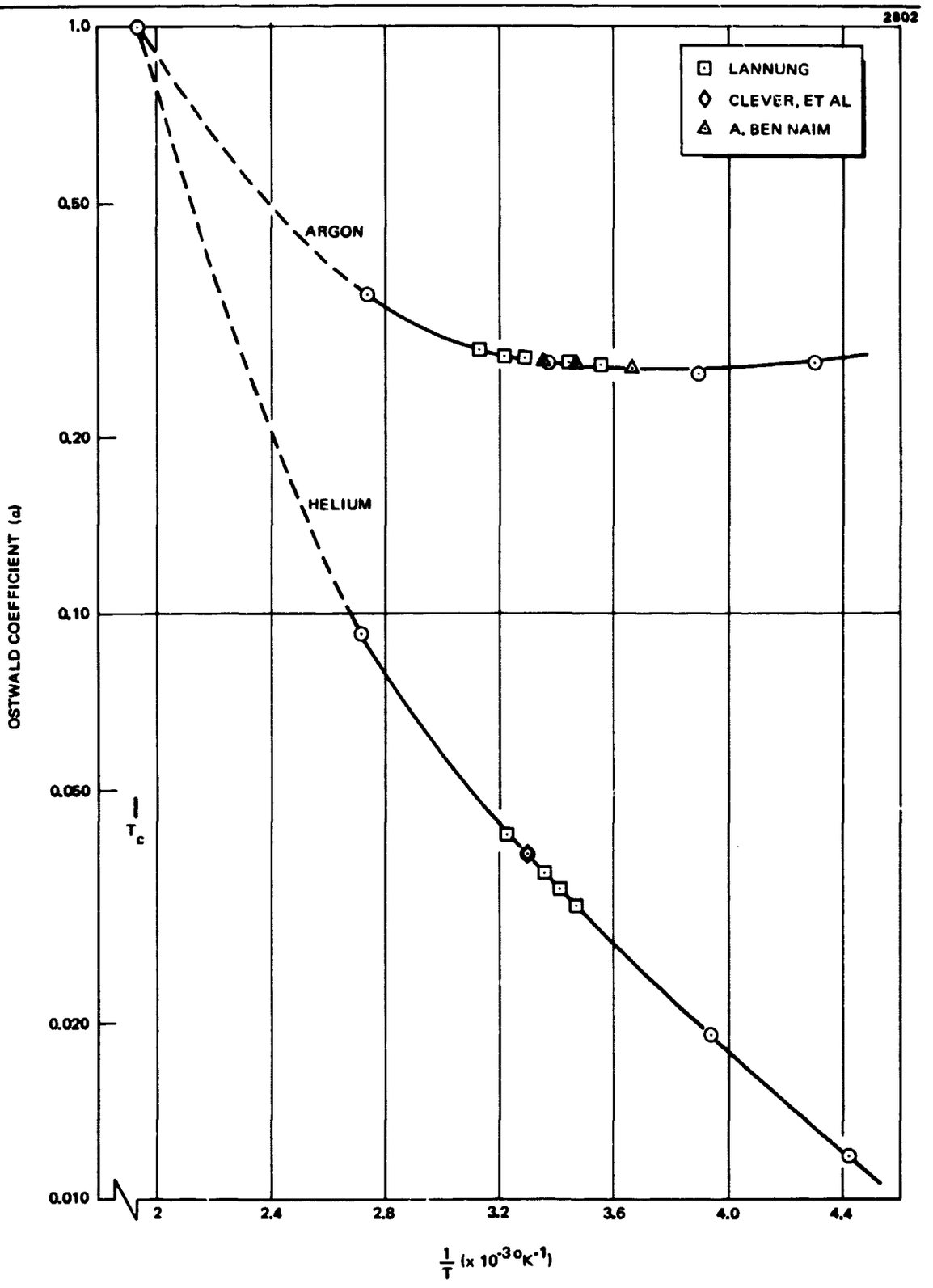

Figure 4-3. Solubility of Helium and Argon in Methanol

Table 4-1

SOLUBILITY DATA SUMMARY

Fluid	Gas	Temperature (°K)	Ostwald Coefficient	Estimated Experimental Uncertainty (%)
Ammonia	He	233	0.00603	*
		253	0.00930	--
		293	0.0280	--
		310	0.0475	--
	Ar	225	0.0416	10
		249	0.0584	5
		291	0.144	5
		310	0.215	10
Freon-21	He	225	0.0138	10
		251	0.0223	5
		297	0.0522	5
		378	0.160	20
	Ar	223	0.0460	5
		252	0.471	5
		299	0.514	5
		375	0.377/0.533	--
Methanol	He	226	0.0117	10
		253	0.0189	5
		303	0.0384	5
		368	0.0918	10
	Ar	232	0.267	5
		257	0.255	5
		297	0.264	5
		365	0.344	10

*Not available. Data from Zakarova (Reference 12).

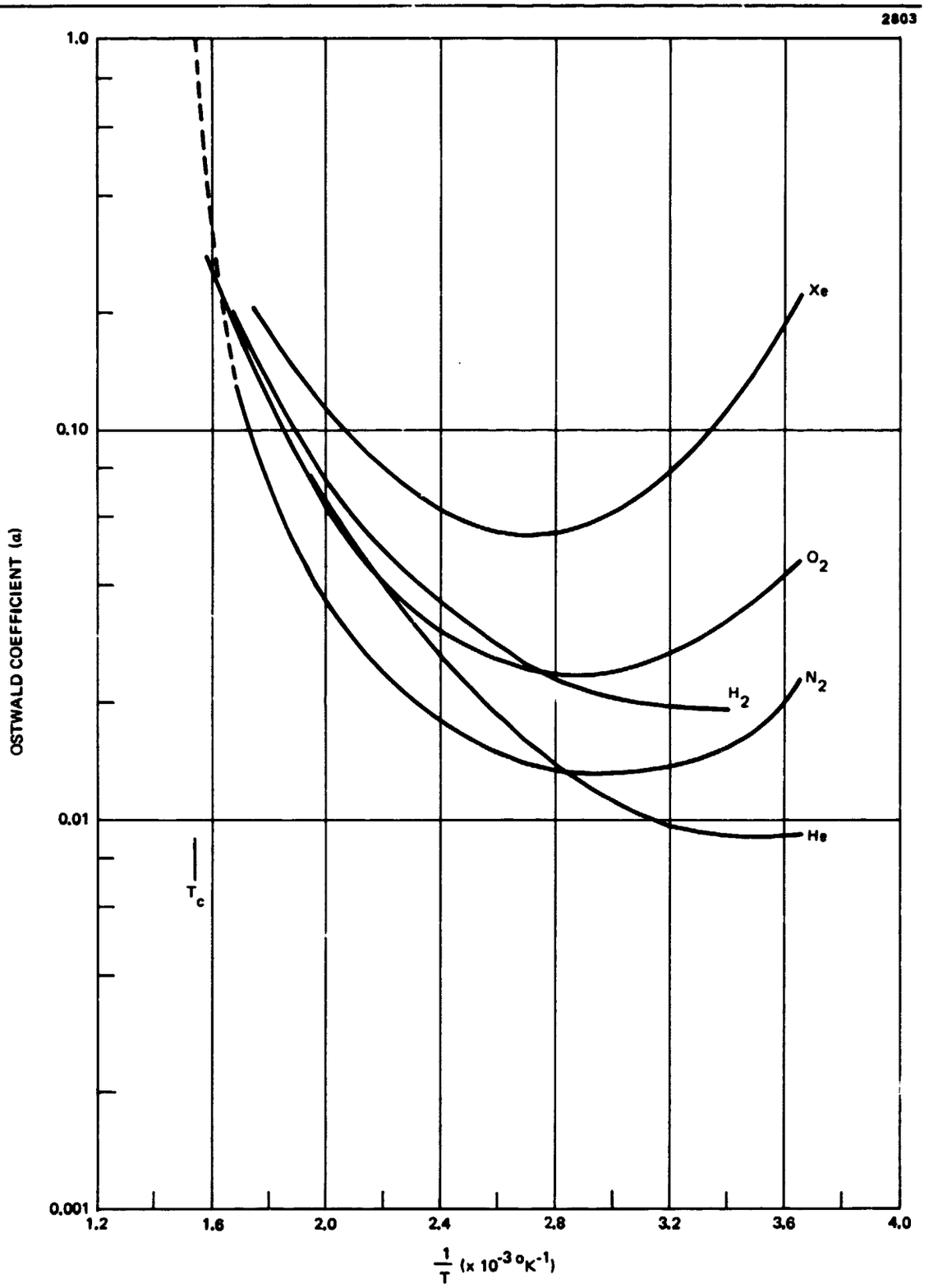

Figure 4-4. Solubility of Various Gases in Water

Diffusion coefficients for the gases and liquids in this program are shown in Figures 4-5, 4-6, and 4-7, and Table 4-2. All were obtained by the collapsing bubble technique with a constant partial pressure of gas internal to the bubble, and degassed fluid. For Freon-21 and methanol, a partial pressure of either 20 or 40 psia was used for all measurements. For ammonia, a 40 psia pressure was used at 20° and 37°C, and 145 psia at the lower temperatures. Pressure-effects influencing diffusion in a liquid should be small at all pressures in this investigation. Included in these results are estimates derived from an empirical equation used frequently in the literature. The Wilke-Change diffusivity equation is given as (Reference 17).

$$D_{ab} = \frac{7.4\,(10^{-8})\,(M_b\psi)^{1/2}\,T}{\mu_b\,V_a^{0.6}} \tag{38}$$

where

D_{ab} = diffusion coefficient, a→b (cm^2/sec)
M_b = solvent molecular weight
ψ = association parameter (water = 2.6, methanol = 1.9, benezene = 1.0, etc.)
T = temperature (°K)
μ_b = solvent viscosity (centipoise)
V_a = molal volume of solute at normal boiling point, (cm^3/g-mole)

Reference 18 gives an empirical relation between the molal volume V_a and the Lennard-Jones parameter σ_a, such that Equation 38 is equivalently given as

$$D_{ab} = \frac{9.76\,(10^{-8})\,(M_b\psi)^{1/2}\,T}{\mu_b\,\sigma_a^{1.8}} \tag{39}$$

Equation 39 has been used with Lennard-Jones parameters from Table A-4 to calculate diffusivity estimates. In general, the Wilke-Chang relationship has not been consistent with experimental data, especially for helium, because it was derived empirically for the diffusion of large solute molecules. As discussed by Nakanishii (Reference 19), helium apparently exhibits quantum mechanical effects, as for example, a higher tunneling probability because of its small size, which enhances diffusion of the gas in solvents. The lack of actual experimental

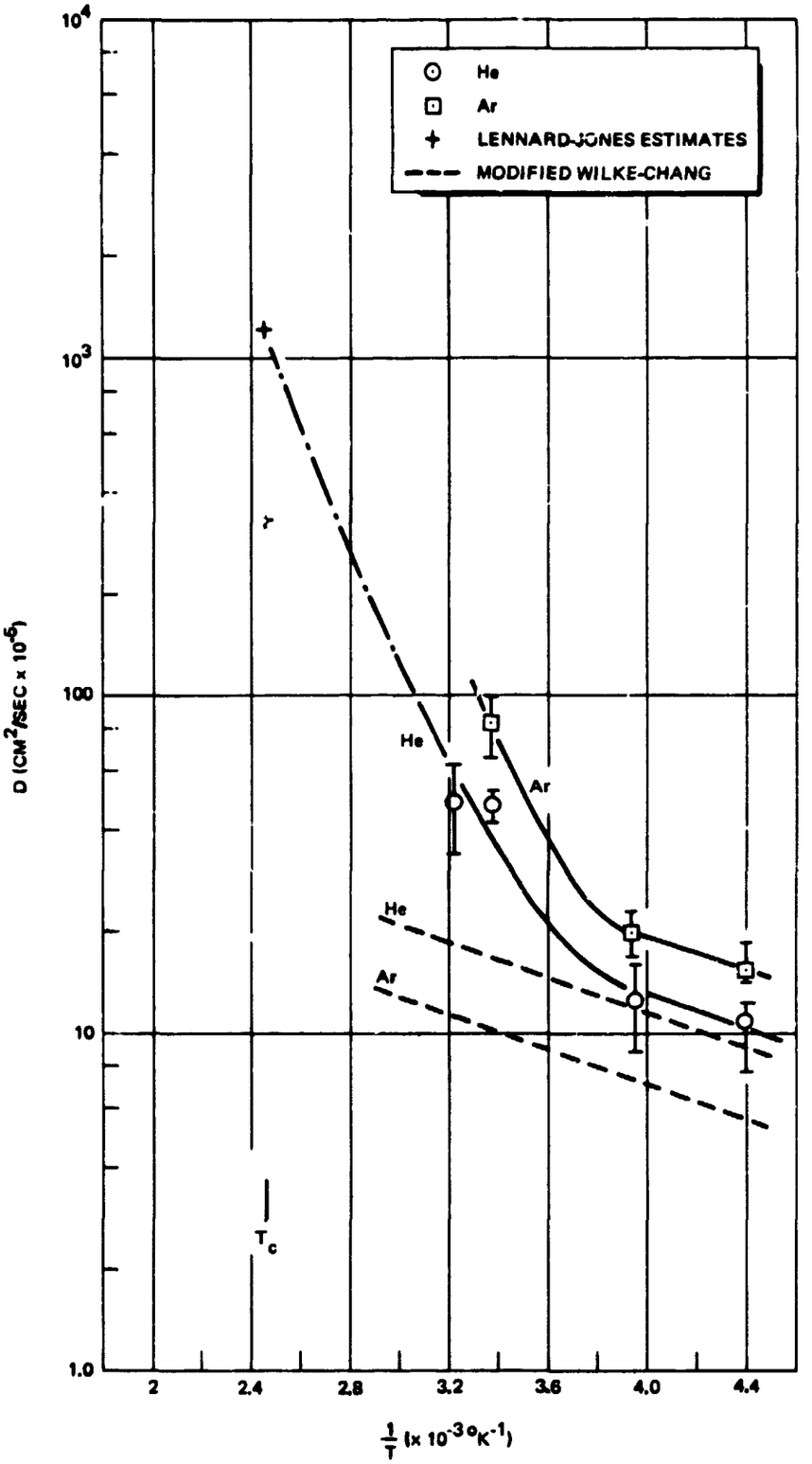

Figure 4-5. Diffusivity of Helium and Argon in Ammonia

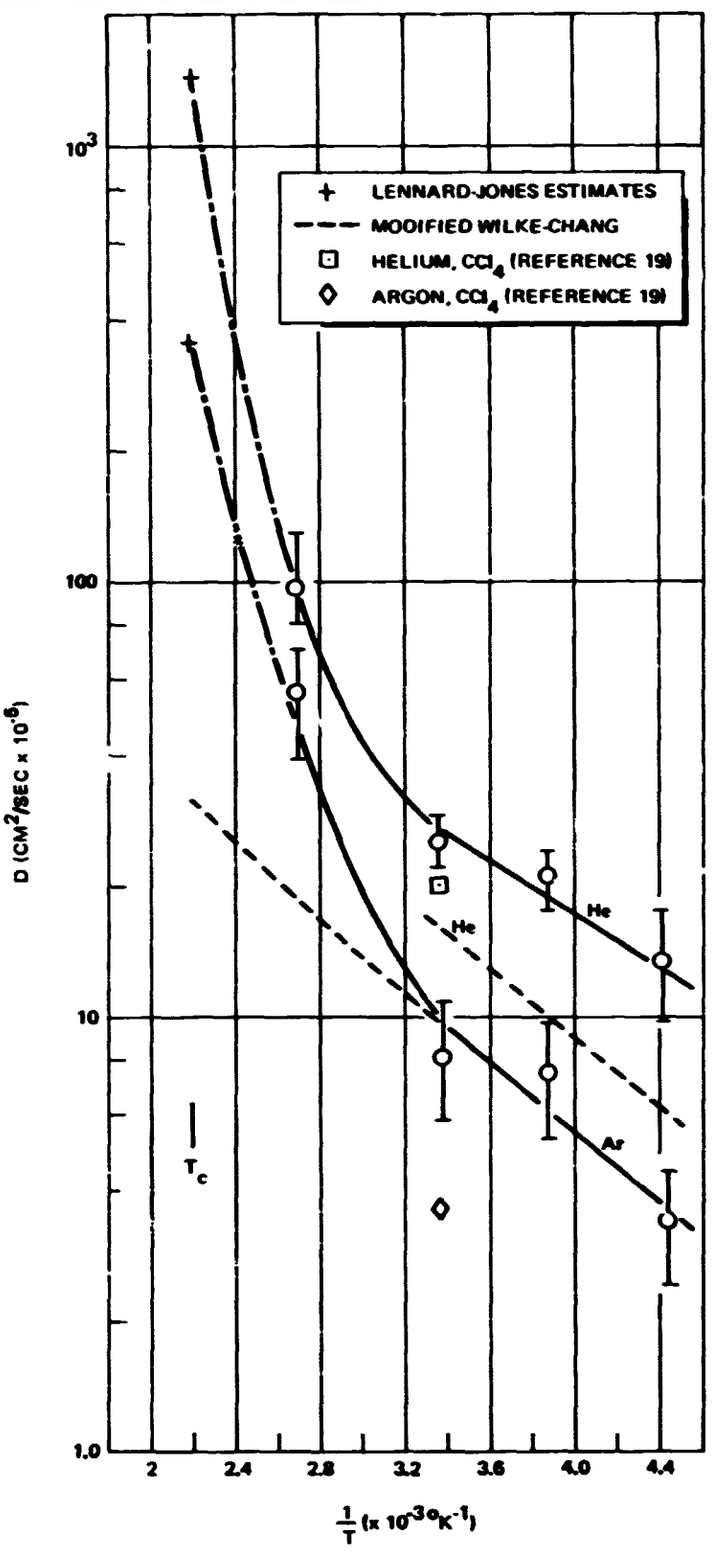

Figure 4-6. Diffusivity of Helium and Argon in Freon-21

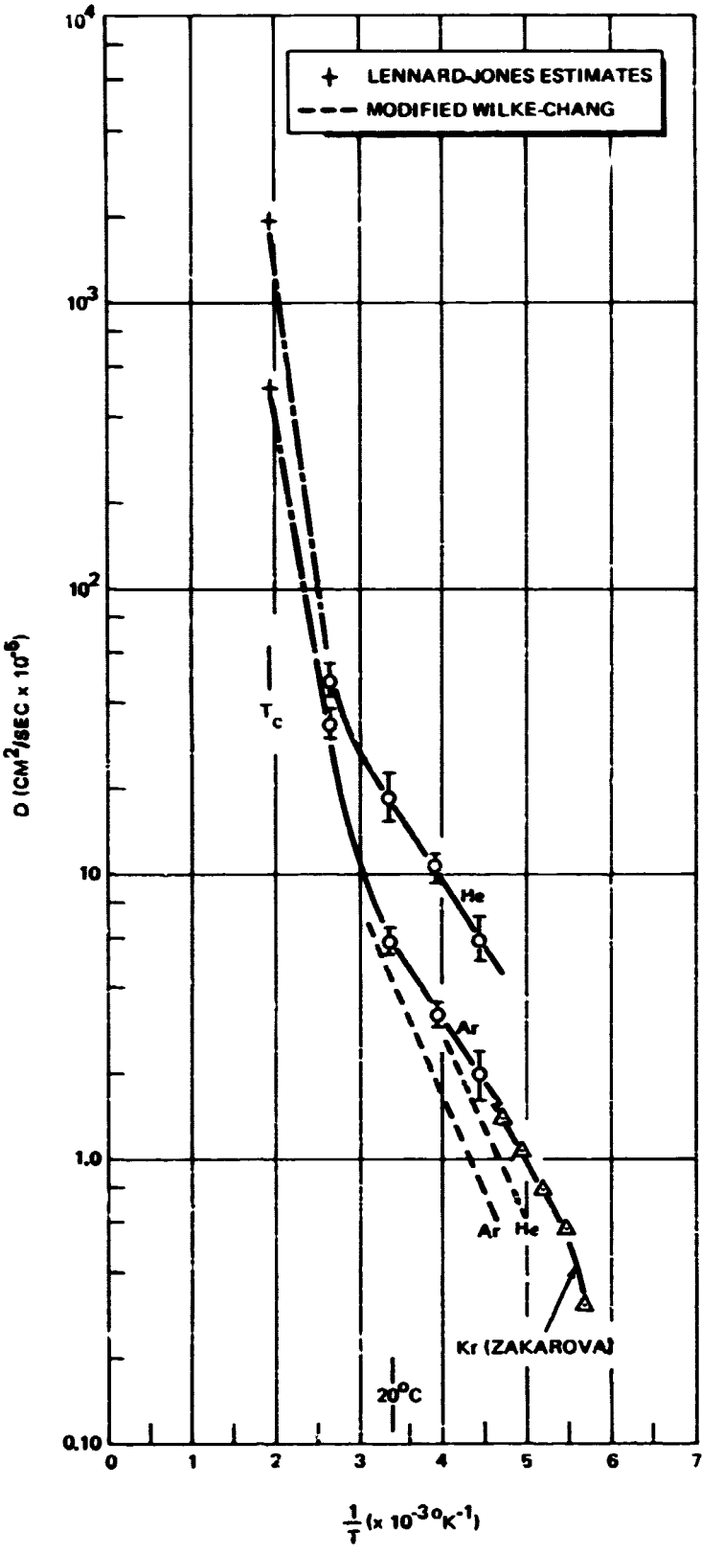

Figure 4-7. Diffusivity of Helium and Argon in Methanol

Table 4-2

DIFFUSIVITY DATA SUMMARY

Fluid	Gas	Temperature (°K)	Diffusivity ($x10^{-5}$ cm^2/sec)	Estimated Experimental Uncertainty (%)
Ammonia	He	227	11.0	30
		254	12.5	30
		296	46.9	15
		310	49.0	30
	Ar	227	15.4	20
		254	19.8	15
		296	82.7	20
		310	*	--
Freon-21	He	226	13.4	30
		258	21.0	20
		297	25.1	20
		370	97.6	40
	Ar	227	3.40	30
		259	7.38	30
		297	8.3	40
		370	56.5	40
Methanol	He	226	5.91	20
		255	10.4	20
		297	16.9	10
		373	47.9	10
	Ar	225	1.99	20
		253	3.24	10
		296	5.83	10
		368	35.9	15

*Beyond limitations of experimental apparatus.

diffusivity data for comparison of values obtained in this program is unfortunate. Data presented here for these fluids with helium and argon may be the first such data ever reported. Data reported by Zakarova (Reference 12) of krypton in methanol is, however, in good agreement with present argon-MeOH data when the small difference in σ_a between these two molecules is considered. Data for argon and helium in CCl_4 are also included in Figure 4-6. The diffusivity of the two gases in CCl_4 should be similar to the diffusivity in Freon-21 because of molecular similarity. The helium-CCl_4 data point is in general agreement with helium-Freon-21 data. Because the argon molecule is much larger than a helium molecule, it can be expected that the Wilke-Chang formula will reasonably predict differences attributable to the physical environment about an argon molecule. If the difference in viscosity for the two fluids is considered in Equation 39, then the diffusivity of argon in Freon-21 is approximately 9.5 (10^{-5}) cm^2/sec, a value in general agreement with the experimental data. At low temperatures, the diffusivity appears to follow the ratio T/μ for the combinations investigated, although absolute values are at variance with Equation 39.

Experimental data indicate a lower diffusivity for helium in ammonia than for argon, at all temperatures. The difference is statistically significant and at present, there is no defect apparent in the measurement technique or data reduction method to account for this anomaly. Additional purification of the ammonia could be attempted, but is not expected to produce a significant change from these results. If the anomaly is real, the explanation may be the significant solvent power of ammonia; ammonia has the unique ability to dissolve alkali and alkaline-earth metals to yield solutions containing solvated electrons. With such solution power, there is possibly some electronic interaction between the argon and ammonia, apart from the Lennard-Jones interaction in which electronic orbitals of the argon molecule are perturbated so as to enhance solubility and diffusivity. The diffusivity of a yet larger molecule, such as xenon, may be of significant value.

At about $T/T_c = 0.60$, all experimental diffusivity data imply a very rapid increase of diffusivity with temperature. Whether this is an artifact of the experimental technique or reflects actual behavior of the diffusion coefficient is uncertain at this time. However, at the critical temperature, the Lennard-Jones gas-gas diffusion coefficient was calculated for the critical pressure,

and the implied trends at lower temperatures are not inconsistent with calculated values, which at the critical temperature, should be considered as approximate, because of the extremely high gas densities. An alternative explanation is a convective current set up by the bubble collapse, which removes solute from the vicinity of the bubble. Whichever explanation is correct, enhanced dissolution at higher temperatures is an experimental fact and should be observable in an arterial heat pipe whenever a bubble rests against a plane surface.

Minimum diffusivity data uncertainty is 10%, maximum is about 40%. Experimental uncertainty of all diffusivity measurements is presented in Table 4-2. The diffusivity measurements are inherently less accurate than the solubility measurements because the analytical technique assumes the solubility is precisely known, which is not correct. In addition, convection currents and small vibration levels can disturb the diffusion field of the collapsing sphere, increasing the dissolution rate and yielding a fictitiously high diffusivity. Diffusivity measurements by this technique are more precise at low temperatures when viscosity is high and convection is minimal, and collapse times are long (>100 sec).

Figures 4-8, 4-9, and 4-10 show the venting parameter $\frac{1}{\alpha D}$ as a function of temperature using the smoothed solubility and diffusivity data estimates. The venting parameter decreases approximately exponentially with temperature below $T/T_c \cong 0.60$ and decreases even more rapidly at higher temperatures. In all cases, the venting parameter of helium is significantly larger than that of argon, as predicted by theory. As the size of the gas molecule increases, the diffusivity decreases as about the square of the molecular diameter (Equation 39), but solubility increases exponentially with molecular diameter, the net result being a decidedly higher venting parameter for helium than for argon, and longer dissolution times for arterial occlusions. The venting parameter of helium in ammonia at low temperature is particularly high, because of very low solubility.

Comparing helium and argon in the three fluids, the combination of helium and methanol has the largest venting parameters for all temperatures, and argon and Freon-21 have the lowest venting parameters of all combinations to about 0°C. From 0° to 100°C, the venting parameters of argon-methanol and helium-Freon-21 are quite similar, but the argon-ammonia combination yields

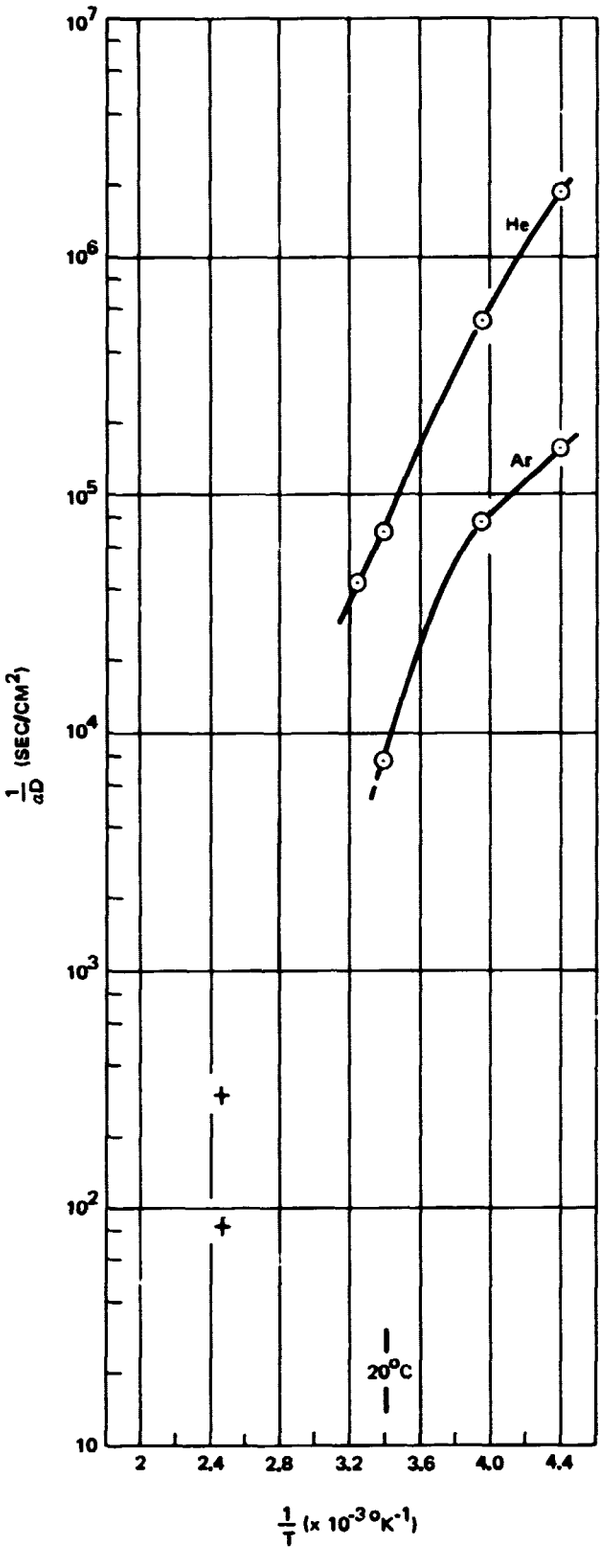

Figure 4-8. Gas Venting Parameter for Helium and Argon in Ammonia

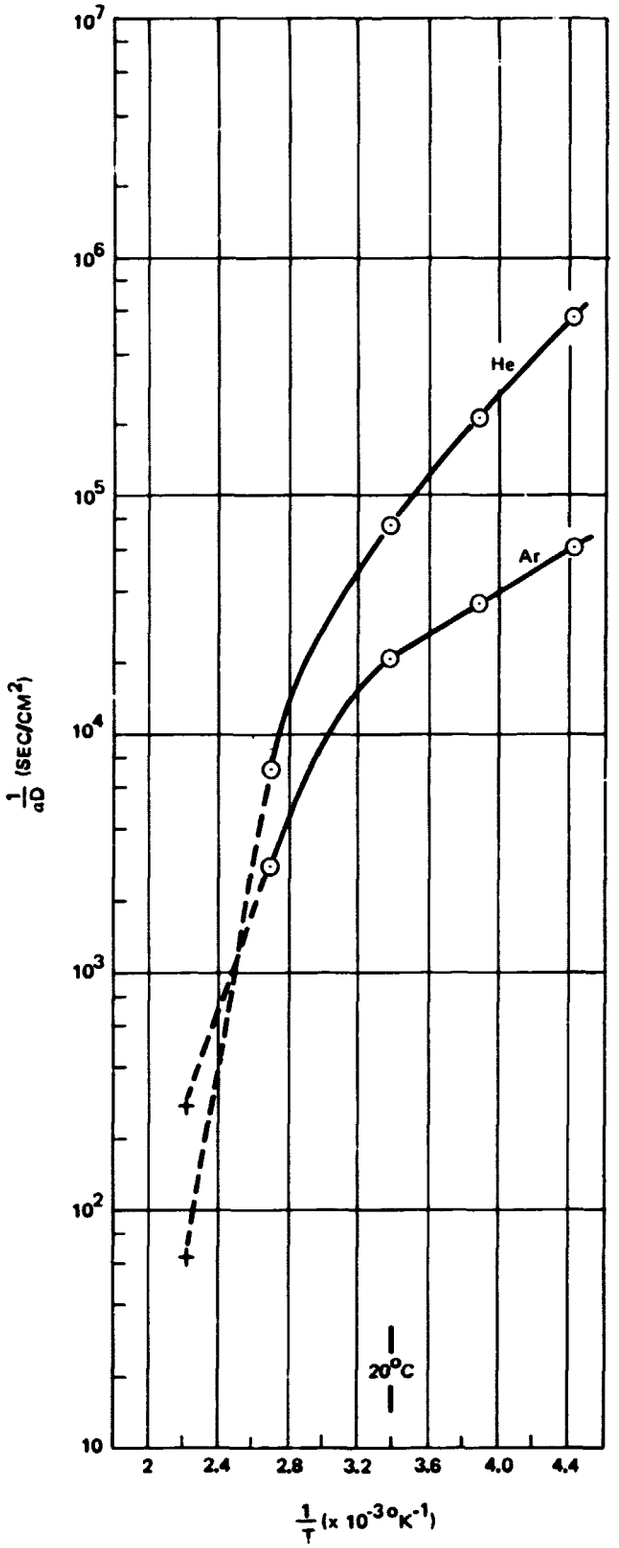

Figure 4-9. Gas Venting Parameter for Helium and Argon in Freon-21

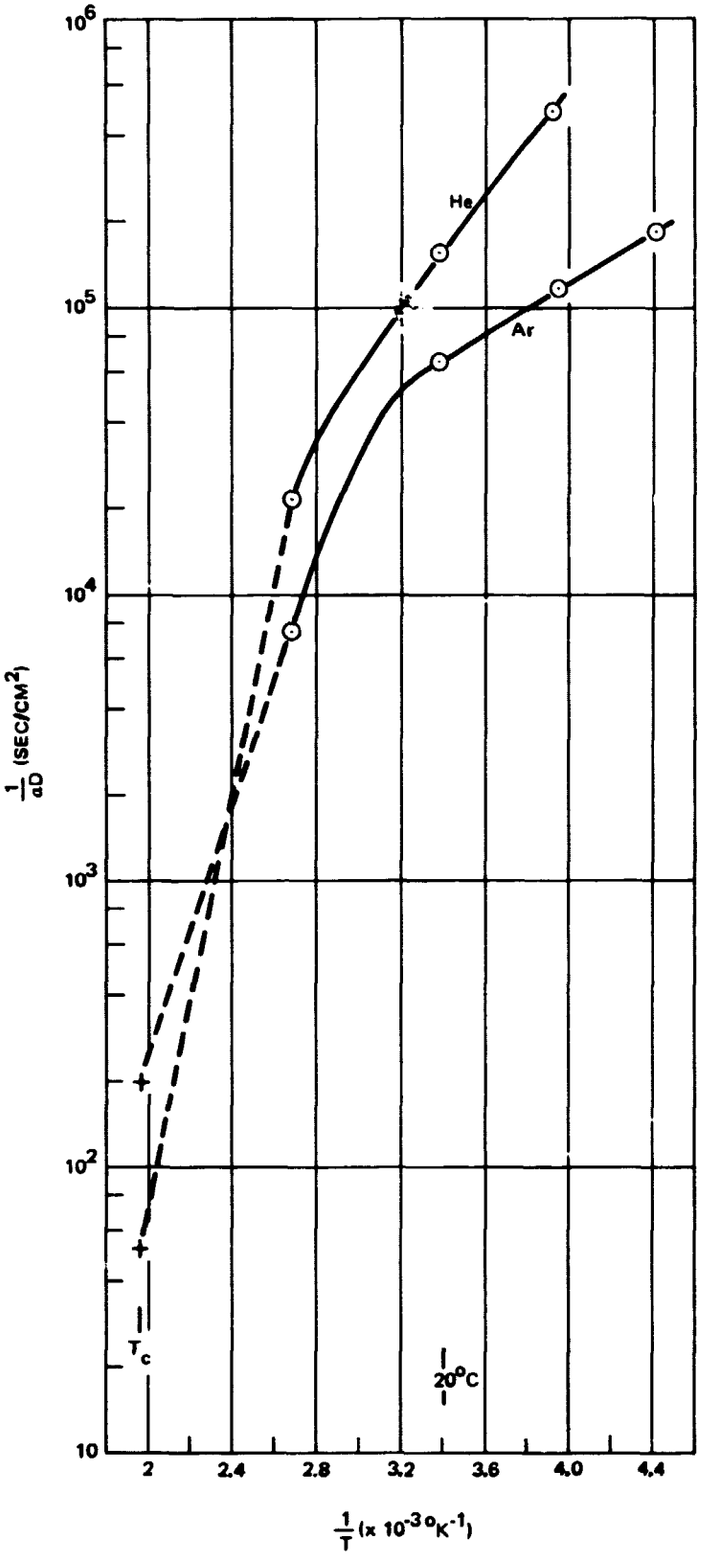

Figure 4-10. Gas Venting Parameter for Helium and Argon in Methanol

the lowest venting parameter and fastest dissolution rate. However, whether or not the pipe is controlled by a noncondensible gas is also of critical importance to selecting a working fluid. Typical venting times for both are shown in Tables 2-1 and 2-2.

4.2 VENTING EFFECTS TESTS

It is desirable for a heat pipe artery to prime after emptying in the presence of noncondensible gas. Possibly the least severe stipulation is artery priming with no heat applied, that is, with the heat pipe isothermal. To experimentally determine the time necessary to effect this refill, arterial simulations were conducted in which known amounts of gas were injected into a heat pipe artery, and the collapse of the occlusion observed as a function of time. The fluids methanol and Freon-21 were used with the gases helium and argon. The test artery was 0.159 cm in I.D., with a wall composed of two layers of 200-mesh square-weave stainless-steel screen. The average wall thickness was 0.0197 cm. The artery had a 4-layer stem of the same screen.

The dissolution of elongated arterial occlusions is discussed first, then the dissolution of spherical arterial bubbles. Spherical-phase observations are appropriate for characterizing isolated spherical bubbles, or spherical bubbles created by the collapse of elongated arterial bubbles.

4.2.1 Dissolution of Elongated Arterial Occlusions

Experimentally, the dissolution of elongated arterial gas occlusions was investigated by charging an arterial simulator (Figure 3-4) with known amounts of noncondensible gas and working fluid. The structure was agitated to ensure an equilibrium between gas in the liquid and vapor, then the screened artery was emptied by tipping and reset horizontal. Collapse of the elongated bubble was recorded as a function of time, temperature, and noncondensible gas (helium or argon). Data presented are for methanol only. Experiments were also run with Freon-21, and results were of the proper magnitude, but data scatter was much less with methanol. This was primarily because of a higher dP/dT with Freon-21 which created a very thermally sensitive system.

The half-life of an elongated bubble is given by Equation 35. The factor (1-f) is equivalently given by

$$1 - f \cong \frac{2\gamma/R_a - \rho g(h_s + 2R_a + \Delta r)}{P_\infty + \frac{2\gamma}{R_a} - \rho g(h_s + 2R_a + \Delta r)} \qquad (40)$$

where

h_s = artery stem height, (cm)
P_∞ = noncondensible gas partial pressure, (dynes/cm^2)
ρ = fluid density, (g/cm^3)

The artery stem height is measured from the fluid surface having infinite radius of curvature. This expression simply is the ratio of the driving pressure to the static pressure within the occlusion. For example, if the stem height is too great, the factor (1-f) will be negative and gas bubble will grow with time.

For purposes of this study, the actual partial pressures of gas used were very low (~1 mm Hg) to obtain reasonable half-lives. The test of Equation 35 was done by calculation of the factor λ as a function of temperature. That is, if Equation 35 is solved for λ, and experimental values are substituted for all other factors, then the model is valid if λ is indeed independent of temperature, and if the value of the tortuosity factor is consistent with some other independent estimator of λ. Figure 4-11 presents the factor λ obtained from experimental half-life data. For all practical purposes, the factor λ is a constant with a value between 0.40 and 0.50. The small but definite increase in λ as temperature decreases has been identified as probably the result of difficulties encountered in measuring the true fluid temperature.

Independently, the optical attentuation factor of a single layer of the screen was measured with an integrating photographic densitometer to be approximately 0.40. The half-life model, therefore, appears to be correct in all essential aspects, and the methanol temperature-dependent venting parameters given in Figure 4-10 are also reasonable. Apparently, a good estimate for λ for open structures such as screening, is the projected free area normal to diffusion, as indicated by satisfactory agreement between the venting characteristic and densitometer measurement. How far this correlation can be carried is not known.

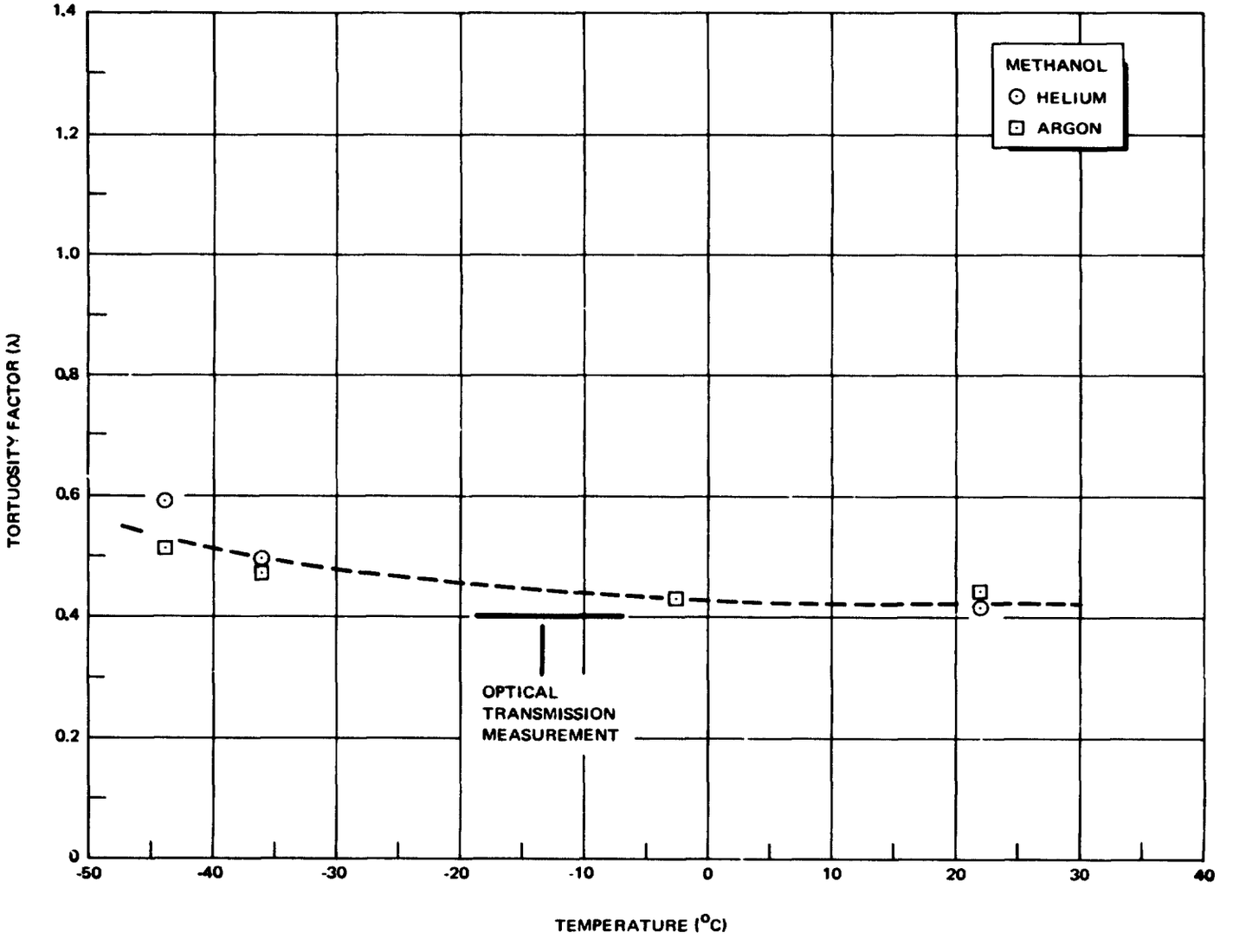

Figure 4-11. Tortuosity Factor Determined from Isothermal Arterial Venting

As an example of half-lifes encountered, with ~1 mm Hg of helium in methanol vapor and a 0.38-cm stem, half-life for an elongated bubble in the 0.159-cm I.D. artery at 22°C was about 1400 sec. Under the same conditions, 3 mm Hg of argon vented with approximately the same half-life, that is, a 32-cm long arterial bubble required about 2 hours to contract to 1 cm in length.

Figure 4-12 shows the limiting collapse behavior of a representative argon bubble as the bubble aspect ratio approaches 1.0. From Equations 33 and 34, the factor β describing the loss rate from the hemispherical end caps must be set equal to 2.25 to describe the data. That is, the loss rate from the end caps is about a factor of 2 over that if the end caps were losing mass into an infinite media. This is occurring because the fluid plug at each end is of finite size, allowing gas to escape to the general vapor environment. The factor β is apparently generally greater than 1.0 for thin-walled arteries, but each arterial design has a different β. Possibly, there is a better means of allowing for end-cap loss than the technique utilized here, where β must be found empirically. However, because the vent time (of an elongated bubble) as given by Equation 34 is only dependent on the logarithm of β, a rather poor choice for the parameter may still yield a reasonable estimate for the vent time. Furthermore, if β is set equal to 1.0, vent time is conservative for a free-standing artery, and is close to actual if the artery were submerged.

4.2.2 Venting of a Spherical Arterial Bubble

The most severe test of the spherical venting model is to predict with some accuracy the venting of a sphere equal in radius to the artery. To maximize the content of this portion of the analysis, assume that the spherical bubble has been produced by the collapse of an elongated bubble, so that the critical factor, the total vent time of an elongated bubble, is given by

$$t_{tot} = t_e + t_s \tag{41}$$

Time t_e is given by Equation 34 and t_s by Equation 32.

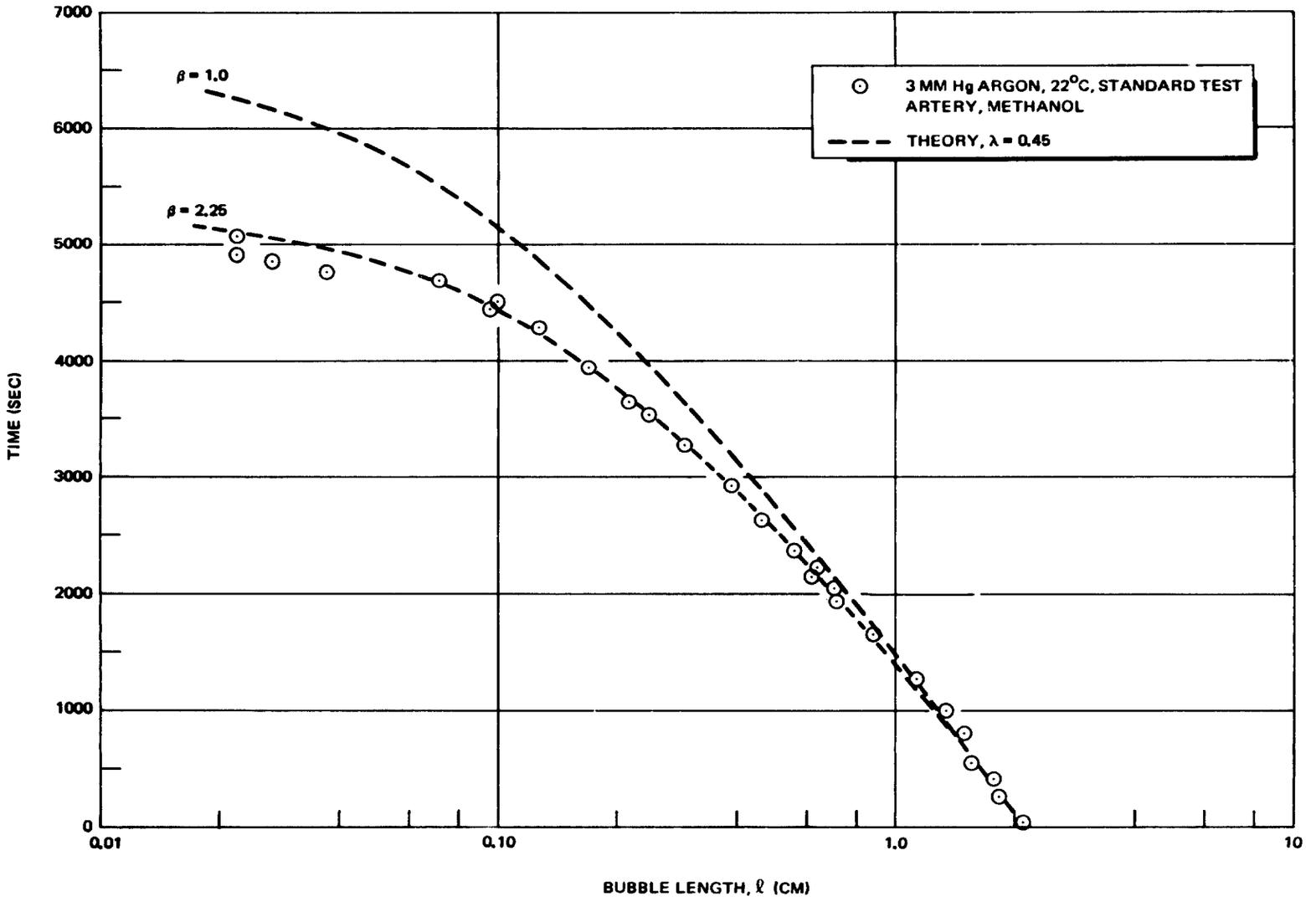

Figure 4-12. Dissolution of an Elongated Arterial Bubble

Figure 4-13 shows the reduced volume of a typical experimentally created occlusion plotted versus time, including the final spherical collapse sequence. Reduced volume is bubble volume divided by $4/3\pi R_a^3$. The total time to dissolve the entire occlusion is 7100 seconds, including collapse time for the spherical phase. The calculated vent time of the spherical phase is 1420 sec, and the total calculated time is about 6800 sec, or about 4% lower than experimental. Both phases appear adequately described by theory to allow engineering calculations of vent time, although the spherical collapse equation used was an infinite media solution, and the environment of the bubble is far from being infinite. However, even if β had been left at the infinite media value, $\beta = 1$, the total vent time from Equation 41 is calculated as 8.150 sec, a value 15% high, but still certainly of the proper magnitude.

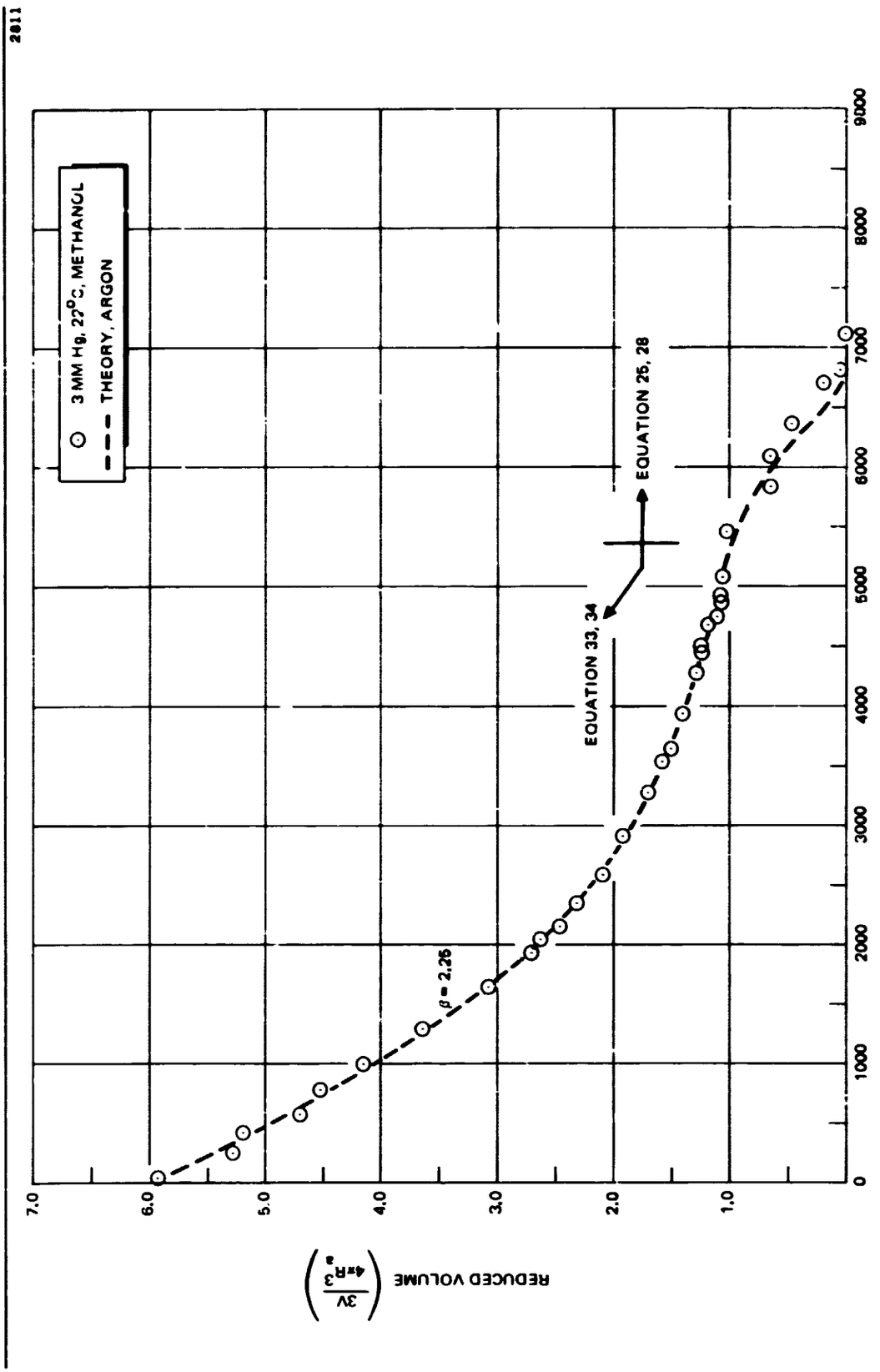

Figure 4-13. Comparison of Calculated and Experimental Total Vent Time for an Elongated Bubble

E

Section 5
CONCLUSIONS

It has been shown both theoretically and experimentally that gas occlusions in arterial heat pipes are a reality. Expressions have been developed giving the lifetime of an arterial bubble under diverse conditions, and these models have been confirmed experimentally, using diffusivity and solubility measurements made in the initial part of this program. These measurements generally cover a field where previous data is nonexistent. However, comparison with theory and with measurements of similar gas-liquid systems confirm most data reported in Section 4.

From measurements of solubility and diffusivity, venting parameters relevant to heat pipe applications have been derived. Under stagnant conditions, trace gas impurities may take from seconds to thousands of seconds to vent, and in heat pipes where noncondensible gases are intentionally introduced, many days may be required for gas occlusions to collapse under particularly unfavorable conditions. The venting studies allow some conclusions concerning minimization of arterial bubble vent time. In terms of physical properties, the ideal fluid is one with high surface tension, low density, and low venting parameter, i.e., inverse solubility-diffusivity product. However, a high surface tension and a high solubility have been shown in Appendix A to be incompatible because solubility decreases with surface tension, so that a fluid with high surface tension, such as water, requires a much longer time to dissolve a gas occlusion than methanol or ammonia. Vent time decreases very rapidly with temperature, because of increasing solubility and diffusivity, so that gas occlusions can be expected to be much more unstable as temperatures increase. It may be feasible to remove gas occlusions in some circumstances by maintaining the heat pipe isothermally at an elevated temperature for some period to take advantage of the lower venting parameter.

The ideal fluid for a gas-controlled heat pipe may have another desirable property, and that is a low vapor pressure. A low vapor pressure working fluid requires a low partial pressure of noncondensible gas, which translates

into a shorter gas venting time. All the venting times measured in this program are quite long, with the highest vapor pressure media, ammonia, requiring the longest time to vent a gas occlusion. The times are all sufficiently long that reliable operation of an arterial gas-controlled pipe may require some dynamic "adjustment" to ensure operation with gas, one being a vapor pressure differential between the gas occlusion and the general vapor space so that the gas is in a state of compression. In that case, ammonia may be a good working fluid because of a high dp/dt.

In summary, the selection of a working fluid requires consideration of a number of factors, including operating temperature, operating mode, and a trade off between good capillary pumping potential and gas venting ability.

In a gas-controlled heat pipe, another option is gas selection. It is desirable to select a gas with a large molecular diameter so as to enhance solution of the gas in the working fluid. At lower temperatures, the effect of gas selection is very apparent.

Some features of an arterial fluid return structure which is resistant to the influence of bubble phenomena can be defined. The diameter of an individual fluid return tube should be small to effect a short vent time. The fluid film between the occlusion and vapor space should be small to produce a rapid mass loss, or the occlusion should be surrounded by fluid flow to accelerate mass transfer. In a gravity field, if the fluid return structure is raised on a stem above the general fluid level, the stem height must not be such that capillary pumping pressure of the hemispherical caps within the artery is expended pumping fluid up to the artery, leaving no pressure differential to create diffusive flow of gas out of the artery.

Section 6
REFERENCES

1. L. E. Scriven, Chem. Eng. Sci., 10, 1 (1959).

2. M. Cable and D. J. Evans, J. Appl. Phys., 38, 2899 (1967).

3. J. L. Duda and J. S. Vrentas, A. I. Ch. E. Jl 15, 351-356 (1969).

4. Carslaw and Jaeger, Conduction of Heat in Solids, Oxford University Press, 247 (1959).

5. P. S. Epstein and M. S. Plesset, J. Chem. Phys., 18, 1515 (1950).

6. J. L. Duda and J. S. Vrentas, Int. J. Heat-Mass Trans., 14, 395 (1971).

7. Forsythe and Wasow, Finite Difference Methods for Partial Differential Equations, John Wiley and Sons, Inc., New York (1960).

8. L. Liebermann, J. A. P., 28, 205 (1957)

9. R. V. Churchill, Fourier Series and Boundary Value Problems, McGraw-Hill, New York (1963).

10. F. Kreith, Principles of Heat Transfer, International Textbook Co., Scranton, Penn. (1967).

11. D. Himmelbau, J. Phys. Chem., 63, 1803 (1959).

12. Zakarova, et. al., Russ. J. Phys. Chem., 43, 3, (1969) (solubility)

13. Lannung, J. Am. Chem. Soc., 52, 68 (1930).

14. Clever, et. al., J. Phys. Chem., 61, 1078 (1957).

15. A. Ben Naim, J. Phys. Chem., 71, 4002 (1967).

16. Himmelbau, J. Phys, Chem., 63, 1803 (1959).

17. C. Wilke, P. Chang, AIChE J., 1, 264 (1955).

18. Bird, Stewart and Lightfoot, Transport Phenomena, Wiley and Sons, 1960.

19. K. Nakanishii, J. Chem. Phys., 42, 1860 (1965).

Appendix A
SOLUBILITY THEORY

A.1 DEFINITION OF SOLUBILITY

The solution of gas into a liquid has received considerable attention, both for economic reasons and because many researchers have felt the dissolution of a gas in a liquid, especially the inert gases, could give information on the physical and chemical structure of liquids. The solubility of a gas in a liquid is experimentally determined by the isothermal mixing of a known amount of gas and a known amount of liquid in a fixed two-phase volume. After some time and agitation, the liquid becomes gas-saturated and an equilibrium between the amount of gas in the liquid and vapor phases is attained. The amount of gas dissolved at constant temperature is directly proportional to gas pressure above the liquid, until gas pressure increases to ~50 to 100 atmospheres. In this discussion, this proportionality constant is expressed as the Ostwald partition coefficient α,

$$\alpha = C_s / Cg \tag{A1}$$

where C_s is the molar concentration of gas in the liquid and Cg is the molar concentration of gas in the vapor phase. This proportionality is more often expressed by Henry's law,

$$P_g = K_h \chi_{g\ell} \tag{A2}$$

The Ostwald coefficient offers several mathematical conveniences. The Ostwald coefficient and Henry's law coefficient K_h are related as

$$\alpha = \rho_\ell RT / (MK_h) \tag{A3}$$

where R is the universal gas constant in appropriate units, M is the molecular weight of the solvent, and ρ_ℓ is the solvent mass density.

For ideal solutions, the Henry's law constant is equal to P_{sg}, the saturated vapor pressure of the "gas" component at the mixture temperature. Under these conditions, Henry's law is known as Raoult's law,

$$P_g = P_{sg} \cdot X_{g\ell} \tag{A4}$$

Deviations from Raoult's law are common, but these deviations decrease as the component mole fraction approaches $x_{g\ell} = 1$, and/or compressibility effects become negligible at low partial pressures of the constituents. At the other extreme, when $x_{g\ell} \leq 0.01$, and/or the gas is above the critical temperature, then Equation A2 is appropriate. For this discussion, Raoult's law is a special case of Henry's law. Most gases discussed here are either below 0.01 mole fraction in the liquids presented, or above the critical point, e.g., helium, argon, and methane. Conversely, liquids are of 0.99 or more mole fraction purity, and are described by Raoult's law. Liquid ammonia, which has a compressibility factor of about 0.7 at room temperature, does not strictly follow these criteria, but this does not affect the calculations which follow.

A.2 NEED FOR A SOLUBILITY MODEL

The removal rate of gas from a bubble is very dependent upon solubility of the gas/liquid pair. Table A-1 lists the Ostwald coefficients for a number of gas/liquid combinations, and shows the tremendous effect of both the gas and liquid on the solubility coefficient. Such a wide range in values at a constant temperature implies correspondingly divergent temperature coefficients, as shown by the data for various gases in water (Section 4.1). Although there are some solubility data from 10° to 30°C for common liquids, there are very little data on the behavior of gas/liquid combinations over an extended temperature range as might be experienced by heat pipes for either terrestrial or aerospace applications. Solubility measurements for all potential gas/fluid combinations are desirable, but without significant expenditure of time and effort, experimental data for the many fluids and gases of interest cannot be derived. With this limitation, understanding of the solution phenomena from a theoretical basis is justified so that attention can be focused on those few gas/liquid combinations which are either unique or represent a broad class of useful liquids and gases.

Table A-1
EXPERIMENTAL SOLUBILITIES AT 25°C FOR A NUMBER OF GASES AND FLUIDS

Liquid	δ	He	Ne	H_2	N_2	Co	O_2	Ar	CH_4	Kr	CF_4	CO_2	Xe	C_2H_6	Rn	C_2F_6
Freon-113	7.2	--	0.099	0.134	--	--	--	0.6200	--	--	0.978		4.3900	5.8300	--	3.05
Ethyl ether	7.4	--	--	0.1300	0.2950	0.3980	0.4660	--	1.0670	--		5.3700	--	--	14.000	--
Freon-21	8.2	0.0525	--	--	--	--	--	0.5130	--	--		--	--	--	--	--
Cyclohexane	8.2	0.0275	0.0419	0.0860	0.1740	--	--	0.3330	0.6630	1.0550	0.233	1.7100	4.5000	--	--	--
CCl_4	8.6	--	--	0.0828	0.1630	0.2240	0.3040	0.3400	0.7240	--	0.301	2.7000	--	5.2700	--	--
Benzene	9.2	0.0210	0.0315	0.0710	0.1230	0.1840	0.2240	0.2400	0.5700	0.7510	0.157	2.6700	3.0800	4.0700	--	0.3040
Acetone	9.3	0.0362	0.0520	0.0769	0.1970	0.2540	0.3080	0.3010	0.7420	--		6.9800	--	--	5.800	--
Chloroform	9.3	--	--	0.0672	0.1360	0.1970	0.2250	--	--	--		3.7000	--	--	13.800	--
Chlorobenzene	9.5	--	--	0.0640	0.1030	0.1520	0.1900	--	0.5000			2.3600	--	3.5200	--	--
Ethanol	12.8	0.0319	0.0455	0.0890	0.1420	0.1930	0.1560	0.2580	--	--		3.2700	--	2.7500	5.700	--
Ammonia	13.7	0.0316	--	0.0722	0.0895	--	--	0.1460	--	--		--	--	--	--	--
Glycol	14.2	--	--	--	0.0153	--	--	0.0370	--	--		--	--	0.2350	--	--
Methanol	14.4	0.0360	0.0486	0.0947	0.1420	0.1960	0.1920	0.2680	0.4280	--		--	--	2.3400	--	--
Water	23.5	0.0097	0.0111	0.0190	0.0156	--	0.0310	0.0343	0.0329	0.0610		0.8300	0.1220	0.0450	0.2240	--
Sodium[1]	28.1	$3.34(10^{-4})$			$3.11(10^{-8})$			$2.27(10^{-5})$		$3.57(10^{-6})$			0.2730			

(1) at 500°C

Table A-2
REFERENCES FOR SOLUBILITY TABLE A-1

Liquid	He	Ne	H_2	N_2	Co	O_2	Ar	CH_4	Kr	CF_4	CO_2	Xe	C_2H_6	Rn	C_2F_6
Freon-113		A17	A6				A6			A15		A17	A6		A6
Ethyl Ether			A3	A3	A3	A3		A3			A4			A16	
Freon-21	P[1]						P								
Cyclohexane	A3	A13	A3	A5			A13	A3	A14	A15	A5	A18			
CCl_4			A3	A3	A3	A3	A1	A3		A15	A1		A1		
Benzene	A3	A13	A3	A1	A1	A3	A3	A3	A1	A15	A1	A18	A1		A6
Acetone	A13	A13	A3	A3	A3	A3	A13	A3			A4			A16	
Chloroform			A3	A3	A3	A3					A4			A16	
Chlorobenzene			A3	A3	A3	A3		A3			A11		A3		
Ethanol	A13	A13	A4	A4	A4	A4	A13				A4		A14	A16	
Ammonia	A2, 12, P		A2, 10	A10			P								
Glycol					A14		A7						A14		
Methanol	A3, P	A13	A3	A3	A3	A3	A13, P	A3							
Water	A8, 9, 13	A8	A8, 9	A8		A8, 9	A7	A9	A8		A8, 9	A8	A9	A8	
Sodium	A19			A19			A19		A19			A19			

[1] Present Investigation

A.3 FUNCTIONAL FORM

The solution of a sparingly soluble gas in a liquid can be addressed using an energy level diagram (Figure A-1). Outside the fluid, the gas has a Maxwellian distribution of energies in the energy levels beginning with $\varepsilon = 0$. Then, on passing through the vapor-liquid interface, molecules must have at least the energy ΔE_1 to break through the fluid surface, but once through, some energy is given back as the gas molecule is bound into the fluid structure. The maximum energy returned is ΔE_2. Because both the gas and liquid are at the same temperature, gas molecules in the fluid still have a Maxwellian distribution of energies, but displaced on the total energy plot by the potential energy difference ΔE_3. If the gas in the liquid phase is in numerical equilibrium with gas in the vapor phase, then it follows that the respective random molecular currents passing through the interface from each direction are equal. The objective is to express these currents mathematically, and in the process, obtain an expression for the Ostwald gas solubility coefficient. Only the molecular current into the fluid is considered in detail because both currents are similarly calculated.

The classical Boltzman distribution for N particles is expressed as (Reference 20)

$$N(\varepsilon)d\varepsilon = \frac{2\pi N}{(\pi KT)^{3/2}} \sqrt{\varepsilon} \exp(-\varepsilon/KT)\, d\varepsilon \qquad (A6)$$

where ε is the kinetic energy, $1/2\ mV_\varepsilon^2$. The incremental molecular current density at a plane perpendicular to an arbitrary x-axis can be expressed as

$$dJ_m = \bar{N}(\varepsilon)V_x(\varepsilon)d\varepsilon d\Omega \qquad (A7)$$

where $N(\varepsilon)d\varepsilon$ is the number density of molecules with energies between ε and $\varepsilon + d\varepsilon$, V_x is the component of velocity toward the interface, and d expresses the intention to sum over solid angle to include all possible orientations with respect to the interface. Physically, the interface is the vapor/liquid interface.

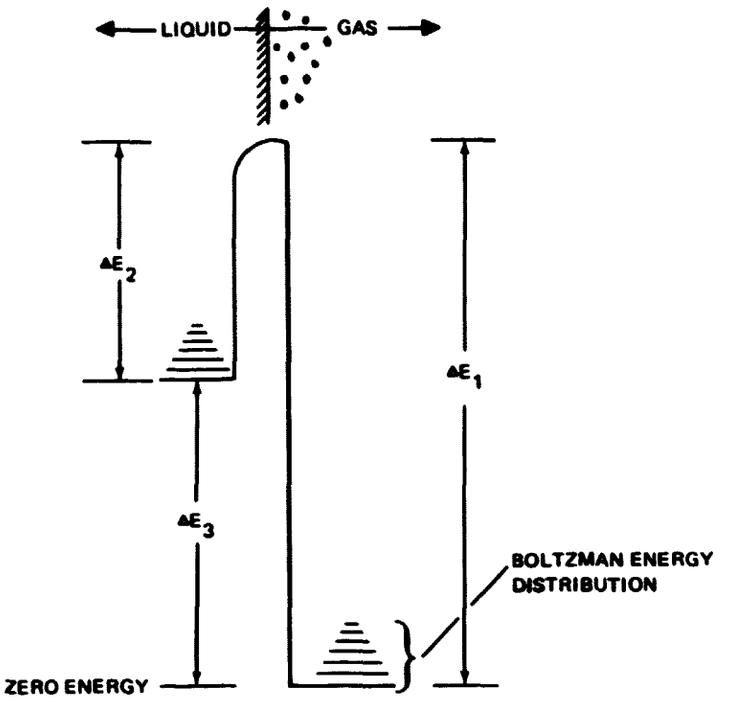

Figure A-1. Energy Level Diagram for Solution Process

The total molecular current density is given by

$$J_m = \int_{\Delta E_1}^{\infty} d\varepsilon \int_0^{\theta_m} \frac{2\pi \bar{N}_{gv}}{(\pi KT)^{3/2}} \sqrt{\varepsilon} \exp(-\varepsilon/KT) \cdot \left(\sqrt{\frac{2\varepsilon}{m_{gv}}} \cos\theta\right) \frac{\sin\theta}{2} d\theta \qquad \text{(A8)}$$

The parenthetic term is the x-directed velocity. The integration in solid angle is performed to an angle θ_m, because there must be sufficient x-directed velocity to break into the fluid. The angle θ_m is then

$$\theta_m = \arccos\left(\sqrt{\frac{\Delta E_1}{\varepsilon}}\right) \qquad \text{(A9)}$$

The angle-integrated current density is

$$J_m = \frac{\pi \bar{N}_{gv}}{\sqrt{2}\,(\pi KT)^{3/2}} \left(\frac{1}{\sqrt{m_{gv}}}\right) \int_{\Delta E_1}^{\infty} (\varepsilon - \Delta E_1) \exp(-\varepsilon/KT) d\varepsilon \qquad \text{(A10}$$

If the variable U is defined as $U = \varepsilon - \Delta\varepsilon_1$, the molecular current is

$$J_m = \frac{\bar{N}_{gv} KT}{(2\pi m_{gv})^{1/2}} \exp(-\Delta E_1/KT) \qquad (A11)$$

A similar analysis of the molecular current from the fluid into the gas phase gives

$$J_m^- = \frac{\bar{N}_{g\ell} KT}{(2\pi m_{g\ell})^{1/2}} \exp(-\Delta E_2/KT) \qquad (A12)$$

Equating the molecular currents,

$$\alpha \equiv \frac{\bar{N}_{g\ell}}{\bar{N}_{gv}} = \left(\frac{m_{g\ell}}{m_{gv}}\right)^{1/2} \exp(-\Delta E_3/KT) \qquad (A13)$$

The Ostwald coefficient α, is exponentially dependent on the difference between the zero-energies of the gas and solution states, and proportional to the square root of the ratios of the masses in the gas and liquid phases. The mass of a gas molecule in the gas phase is the usual mass, although the effective mass of the molecule in the liquid can be greater because of intermolecular bonds. For practical purposes, the square root ratio can be included in the exponential, and a new effective energy difference $\Delta E_3'$ defined as

$$\alpha = \exp(-\Delta E_3'/KT) \qquad (A14)$$

where $\Delta E_3' = \Delta E_3 + 1/2\, \ell n \left(\frac{M_{g\ell}}{M_{gv}}\right)$

The expression for α in Equation A14 is identical with expressions for α in References A21 and A22, where the final form was approached from thermodynamic methods.

Reference A23 gives a statistical mechanical solution for α for a hard sphere fluid in the form of Equation A13, where the pre-exponential factor is defined as

$$\left(\frac{m_{g\ell}}{m_{gv}}\right)^{1/2} = 1/(1-y) \qquad (A15)$$

and y is defined as the ratio of the hard-sphere fluid volume to the true volume; y has a value of about 1/2 for many fluids.

A.4 SOLUBILITY MODELS

It is common practice to separate the energy difference ΔE_3 into components ΔE_1 and ΔE_2 (Figure A1). Energy ΔE_1 represents the energy to get a molecule into a suitable site in the fluid, while ΔE_2 results from the attraction of the solute molecule by the solvent molecules. Recent efforts have centered around different mathematical models for ΔE_1 and ΔE_2. Discussion of the models here emphasizes utility in predicting solubility coefficients of various gases and liquids over a wide temperature range. Table A-3 presents the efficiency of the various models in correlating and predicting solubilities of a number of gases and liquids. For each liquid, the various models are least squares fitted to available data as given in Table A-1, for 25°C, and then the degree of fit is compared. The accuracy of each model is presented by the ratio of the summed square deviations about the model, divided by the summed square deviations about the average value of the data for a given fluid at 25°C, subtracted from one

$$r = 1 - \frac{\sum_{n=1}^{m} (Y_n - g(x, z))^2}{\sum_{n=1}^{m} (Y_n - \overline{Y})^2} \qquad (A16)$$

The function g(x, z) represents the theoretical estimate to the nth data point, y_n. A value r = 0, implies the model is no better than a simple average of the input data, while r = 1 implies a perfect fit of the data. When N = 2, r equals one for a one-parameter theory with non-zero intercept, regardless of the model. In that as well as other cases, it is equally important to compare model effectiveness in predicting solubility data over the -50° to 100°C temperature range of this program for methanol, Freon-21, and ammonia, with argon and helium. This comparison is discussed later.

What follows is a summary of the models used in this comparison, presenting the essential details of each. Energy ΔE_2 is calculated with Lennard-Jones potential parameters by most investigators, while the characterization of ΔE_1 has been more diverse. Discussion of ΔE_2 will be deferred until the various expressions for ΔE_1 are established.

Table A-3

SOLUBILITY MODELS FITTED TO DATA

Fluid	M, gases fitted	Model 1			Model 2			Model 3		
		C_1	C_2	r_1	C_1	C_2	r_2	C_1	C_2	r_3
Freon-113	5	1.23	0.610	0.999	2.12	0.720	0.9999	1.16	1.16	0.999
Ethyl ether	7	1.37	0.727	0.983	1.97	0.790	0.975	0.738	1.28	0.948
Freon-21	2	1.54	0.655	1.00	2.28	0.744	1.00	0.776	1.27	1.00
Cyclohexane	9	0.973	0.721	0.989	1.27	0.777	0.985	0.511	1.46	0.924
CCl_4	8	0.929	0.639	0.989	1.20	0.682	0.983	0.443	1.25	0.900
Benzene	12	1.10	0.677	0.983	1.63	0.764	0.971	0.987	1.29	0.931
Acetone	10	1.43	0.536	0.910	2.40	0.631	0.870	1.31	0.950	0.851
Chloroform	6	1.15	0.689	0.984	1.54	0.740	0.979	0.629	1.27	0.941
Chlorobenzene	7	0.860	0.559	0.976	1.26	0.625	0.970	0.973	1.05	0.936
Ethanol	10	1.52	0.554	0.957	2.23	0.631	0.942	0.853	1.04	0.913
Ammonia	4	2.84	0.353	0.851	5.11	0.489	0.357	1.51	0.644	0.500
Methanol	9	1.36	0.404	0.975	2.24	0.496	0.930	1.16	0.739	0.918
Water	12	1.06	0.178	0.958	1.58	0.222	0.873	1.22	0.330	0.861
Average variance reduction - 101 gas/liquid combinations				0.966			0.910			0.894

Definitions:

r_i = fraction reduction in log-solubility variance for the i^{th} model, defined by

$$r_i = 1 - \frac{\sum_{n=1}^{M} (\ell n(\alpha_n) - (C_1 E_1 + C_2 E_2))^2}{\sum_{n=1}^{M} \left[\ell n(\alpha_n) - \bar{y} \right]^2}$$

and $$\bar{y} = \frac{1}{M} \sum_{n=1}^{M} \ell n(\alpha_n)$$

C_1, C_2 = least-squares fitting coefficients necessary to minimize variance.

Model solubility equation for a given fluid is then

$$\ell n(\alpha) = -\left[C_1 E_1 / KT + C_2 E_2 / KT \right],$$

where E_1, E_2 are given as

Model 1, E_1 = Eq A17, E_2 = Eq A30

Model 2, E_1 = Eq A19, E_2 = Eq A30

Model 3, E_1 = A21, E_2 = A30

A.5 SURFACE TENSION MODEL

Energy ΔE_1 was first interpreted by Uhlig in 1937 (Reference 24) as the work necessary to produce, against surface tension, a spherical hole in the fluid large enough to fit a spherical solute module of radius r. This is

$$\Delta E_1 = 4\pi\gamma r^2 \tag{A17}$$

References A21 and A26 are more recent examples of approaches using this model for ΔE_1. A defect of this model is that γ changes as r approaches molecular dimensions, so that, the effective surface tension is actually a function of r. In addition, a small molecule can fit between the solvent molecules in interstital positions with less energy expenditure than given by Equation A17. If the fluid is considered as an assemblage of hard spheres of diameter σ_b, and the experimental number density of fluid molecules is ρ_b, then the interstital holes can be treated as an internal lattice of small vacant spheres with equivalent radius r_o,

$$r_o = \left[\frac{3(1-y)}{4\pi\rho_b}\right]^{1/3} \tag{A18}$$

where $y = \frac{\pi}{6}\rho_b \sigma_b^3$

The quantity (1-y) is the fractional free volume in a fluid with molecules of hard-sphere diameter σ_b. The energy ΔE_1 is then given by

$$\Delta E_1 = 4\pi\alpha(r^2 - r_o^2) \tag{A19}$$

A.6 SCALED PARTICLE MODEL

By the method of scaled particles, Reiss et al., (Reference 23) derived an expression for the amount of work required to insert a sphere of zero radius into a hard sphere fluid,

$$\Delta E_1 = -KT\,\ell n\,(1-y), \qquad (r = \sigma_b/2) \tag{A20}$$

The radial coordinate in this analysis is taken from the center of a solvent molecule. For solute molecules of non-zero size, Equation A20 was expanded in a power series in this coordinate system as

$$\Delta E_1(r) = K_o + K_1 r + K_2 r^2 + K_3 r^3 \tag{A21}$$

where $r = (\sigma_a + \sigma_b)/2$ and σ_a is the solute molecule diameter. In the limit of large r, macroscopic thermodynamics is valid, making it possible to express the polynomial coefficients in terms of known physical properties from the limits of both zero and very large r_a. The coefficients are

$$K_o = KT\left(\frac{\sigma_a}{2}\left(\frac{Y}{1-Y}\right)^2 - \ln(1-Y)\right) - \frac{\pi P \sigma_a^3}{6} \quad \text{(A22)}$$

$$K_1 = \frac{-KT}{\sigma_a}\left(18\left(\frac{Y}{1-Y}\right)^2 + \frac{6Y}{1-Y}\right) + \pi P \sigma_a^2 \quad \text{(A23)}$$

$$K_2 = \frac{KT}{\sigma_a^2}\left(18\left(\frac{Y}{1-Y}\right)^2 + \frac{6Y}{1-Y}\right) - 2\pi P \sigma_a \quad \text{(A24)}$$

$$K_3 = \frac{4}{3}\pi P, \quad \text{(A25)}$$

where P is the macroscopic pressure above the liquid.

Experimental data indicate that Equation A20 significantly underestimates the work to insert small gas molecules into a real fluid. However, when the model is corrected by least-squares fitting to data at a single temperature, the temperature-dependent solubility then predicted agrees well with some data.

A. 7 SOLUTION THEORY

Hildebrand and Scott (Reference 25) expressed $(\Delta E_1 - \Delta E_2)$ in terms of a differential heat of vaporization. Their final expression for solubility is

$$\ln x_a = \ln x_a^i - \left[\frac{\overline{V}_a}{RT}\left(\delta_b^2 - \delta_a^2\right) + \ln\left(\frac{\overline{V}_a}{V_b}\right) + \left(1 - \frac{\overline{V}_a}{V_b}\right)\right] \quad \text{(A26)}$$

In this equation, x_a denotes the solubility in mole fraction, x_a^i equals the Raoult's Law solubility, $\overline{V}_a$ the partial molar volume of the solute in the solvent, and V_b the molar volume of the solvent. The parameter δ for the i^{th} component is

$$\delta_i^2 = \frac{h_{fgi} - RT}{V_i} \quad \text{(A27)}$$

F

The factor δ is called a solubility parameter, and this value in $(\text{calories/cm}^3)^{1/2}$ is included in Table A-1 for the fluids presented. Fluid solvency is ranked by this solubility parameter, and solubility of a given gas roughly follows the solubility parameter of the fluid as in Equation A26.

To use Equation A26, one vapor pressure, two heats of vaporization, and two molar volumes are needed. In some cases, the last two terms contribute little and are neglected, but this still requires considerable property data. In addition, other solubility models are as accurate, require less property information, and have the same exponential/pre-exponential format. For these reasons, this model is not considered further.

A.8 LENNARD-JONES MODEL FOR ΔE_2

The negative work term ΔE_2 is customarily described by the Lennard-Jones potential. The Lennard-Jones pair potential (LJP) is

$$\mu(r) = 4\epsilon \left((\sigma/r)^{12} - (\sigma/r)^6 \right) \tag{A28}$$

where σ and ϵ are parameters describing the interaction potential of finite-sized non-polar molecules. If, as in the case of physical absorption, a molecule is surrounded by several others, the total energy of interaction is the sum of the individual interactions of the solute molecule with the solvent lattice molecules. This sum can become an integral if the number of molecules is known as a function of position with respect to the solute molecule. The number of molecules in a spherical shell of thickness dr at a radial distance r is given by the radial distribution function g(r) as

$$n(r, r+dr) = \rho_b \, g(r) \, 4\pi r^2 \, dr \tag{A29}$$

The distribution function for a Lennard-Jones mixture has, however, not been derived, and approximations must be made. One of the most used simplifications (and possibly least exact) is to smooth the interaction by giving the solvent continuum properties and integrating the LJP over all space from the solvent-solute closest approach distance to infinity.

$$\Delta E_2 = -16\pi \rho_g \bar{\epsilon} \int_{\bar{\sigma}}^{\infty} r^2 \left((\tfrac{\bar{\sigma}}{r})^{12} - (\tfrac{\bar{\sigma}}{r})^6 \right) dr = \frac{32}{9} \pi \rho_g \bar{\epsilon} \bar{\sigma}^3 \tag{A30}$$

The barred terms are mean values of the respective parameters because the interaction is not between likes. The various symbols are

ΔE_2 = LJP interaction energy (ergs)
ρ_b = solvent molecular density (cm^{-3})
$\bar{\epsilon}$ = mean energy parameter = $(\epsilon_a \epsilon_b)^{1/2}$ (ergs)
σ = molecular approach parameter = $1/2\ (\sigma_a + \sigma_b)$ (cm)
a, b = gas, liquid, respectively

To account for the interaction of a polar fluid with a nonpolar (but polarizable) gas, the following parametric corrections are suggested by Reference A22.

$$\bar{\epsilon} = (\epsilon_a \epsilon_b)^{1/2} \cdot p^2 \qquad \text{(A31)}$$

$$\bar{\sigma} = 1/2\ (\sigma_a + \sigma_b)/p^{1/6} \qquad \text{(A32)}$$

$$\rho = 1 + \sqrt{\frac{2}{2}}\ \frac{\alpha_a\, t_b^*\, \sqrt{\epsilon_b/\epsilon_a}}{\sigma_a^3} \qquad \text{(A33)}$$

where

ρ = polarization factor
α_a = polarizability of non-polar molecule (cm^3)
t_b^* = fluid polarization parameter (tabulated)

Equation A30 provides a means for ranking various gases in terms of solubility. Solubility is exponentially dependent on the factor $\epsilon_a\ \sigma_a^{3/2}$ and this means of ranking the gases has been used in Table A-1. Except for the fluorinated hydrocarbon gases, this factor describes relative solubility well for a given fluid.

A.9 SOLUBILITY CALCULATIONS

The models for ΔE_1 and ΔE_2 relate solubility to surface tension, heat of vaporization, and potential and geometrical factors on a molecular basis. As discussed earlier, these models and the ability to predict data are presented in Table A-3. Lennard-Jones parameters are summarized in Tables A-4 and A-5, and are principally from References A26 and A27. Viscosity-derived potential parameters were used because the more appropriate second-virial coefficient values are less abundent from various investigations and more

Table A-4

LENNARD-JONES PARAMETERS FOR GASES

Gas	σ (Å)	ϵ_o/K(°K)	α_a($\times 10^{-24}$ cm^3)
Helium	2.57	10.8	0.2040
Neon	2.858	27.5	0.393
H_2	2.915	38.0	0.802
Nitrogen	3.798	71.4	1.730
CO	3.706	88.0	1.930
Oxygen	3.433	113.9	1.560
Argon	3.405	121.2	1.630
Methane	3.796	144.0	2.700
Krypton	3.621	171.6	2.460
CF_4	4.660	134.0	2.860
CO_2	4.185	189.6	2.590
Xenon	4.055	229.0	4.000
Ethane	4.380	236.0	4.330
Radon	4.390	270.0	6.300
C_2F_6	5.320	186.0	

Table A-5

LENNARD-JONES PARAMETERS FOR LIQUIDS

Fluids	σ,(Å)	ϵ_o/K (°K)	t^*
Freon-113	5.66	496.0	
Ethyl Ether	5.678	314.0	
Freon-21	5.093	296.4	0.1
Cyclohexane	6.182	297.0	
Carbon Tetrachloride	5.947	322.7	
Benzene	5.350	412.0	
Acetone	4.600	560.0	0.7
Chloroform	5.389	340.0	0.1
Chloro-benzene	5.610	610.0	
Ethanol	4.530	362.6	
Ammonia	2.900	558.0	1.0
Methanol	3.626	482.0	0.8
Water	2.6410	809.0	1.2
Sodium	3.840	1970.0	

often of conflicting size. The Lennard-Jones parameters σ_a and σ_b are assumed to be the equivalent hard-sphere diameters of the solute and solvent molecules, respectively.

For the surface tension model, the equilibrium radius was taken as $(2)^{1/6}\ \sigma_{ab}$, in accordance with findings that the radial distribution function of a pure Lennard-Jones fluid has a peak at the potential minimum, $\mu = \varepsilon/K$[7, 10]. In the second version of this model, work against the fluid was assumed to be only the surface-tension work to enlarge an interstital hole to the final radius. A temperature-dependent surface tension was used, as suggested by Reference A28.

$$\frac{\alpha_1}{\alpha_2} = \left(\frac{1-T_{r1}}{1-T_{r2}}\right)^n \qquad \text{(A34)}$$

where T_{r1} and T_{r2} are the reduced temperatures with respect to the critical point. For the organic fluids, n was set equal to 1.2. The following values of n were found to describe $\alpha(T)$ best by Equation A34 for the fluids in this program:

Methanol, n = 0.90
Freon-21, n= 1.22
Ammonia, n= 1.22

The number density of solvent atoms as a function of temperature was derived from a generalized equation for liquid density by Yen and Woods (Reference A30). Yen and Woods ascribe a maximum error of 2.1% for 62 pure fluids. In a check of equation accuracy, the density of Freon-21 was calculated within 0.25% of experimental data, from -40° to 50°C.

The least squares model used to compare the theories is based on the natural logarithm of the solubility values, because the functional form of the solubility is exponential in ΔE_1 and ΔE_2. A function of the form

$$\ln \alpha = -\left(C_1 \frac{\Delta E_1}{KT} + C_2 \frac{\Delta E_2}{KT}\right) \qquad \text{(A35)}$$

was used to fit the data. If the reduction in variance r is 1.0, and C_1 and C_2 are both 1.0, then the theory exactly describes the experimental data, and ΔE_1 and ΔE_2 are statistically correct. Unfortunately, none of the models are correct in that detail.

All methods are fairly good estimators of solubility. The model best describing data at 25°C is the Uhlig model (Reference A24) utilizing surface tension, the least accurate is the scaled-particle model using a complex polynominal expression. However, neither surface tension model predicts experimental data as well as Model 3 over the entire temperature range investigated.

The ability of each model to predict solubility temperature-dependence was determined as follows. For each fluid, the adjusting coefficients to theory, C_1 and C_2, were calculated so that the solubilities of helium and argon were given exactly at 25°C. Then, the solubility at all other temperatures was calculated using the same coefficients in Equation A25, that is, if the models are fundamentally correct, the adjusting coefficients change little with temperature and experimental data is well represented by the theoretical estimates. Figures A-2 and A-3 show the behavior predicted by the various models for argon and helium in Freon-21 and methanol.

The solubility of helium and argon in Freon-21 is well represented by scaled-particle theory, but the solubility of helium and argon in methanol is not described well by any of the models. In all cases, the surface tension models are poor estimators of solubility as a function of temperature. Although the scaled particle technique reproduced the Freon-21 data well, it did not reproduce the methanol data, and the reason for this is not clear. The usefulness of the various models lies primarily in the domain of identifying important physical properties, such as surface tension, which relate solution of a gas to other important heat pipe characteristics, such as capillary pumping capabilities.

A.10 SUMMARY

The solubility of gases in liquids has been presented from a theoretical standpoint, with moderate success in predicting solubility as a function of temperature. The agreement is adequate to enable identification of physical

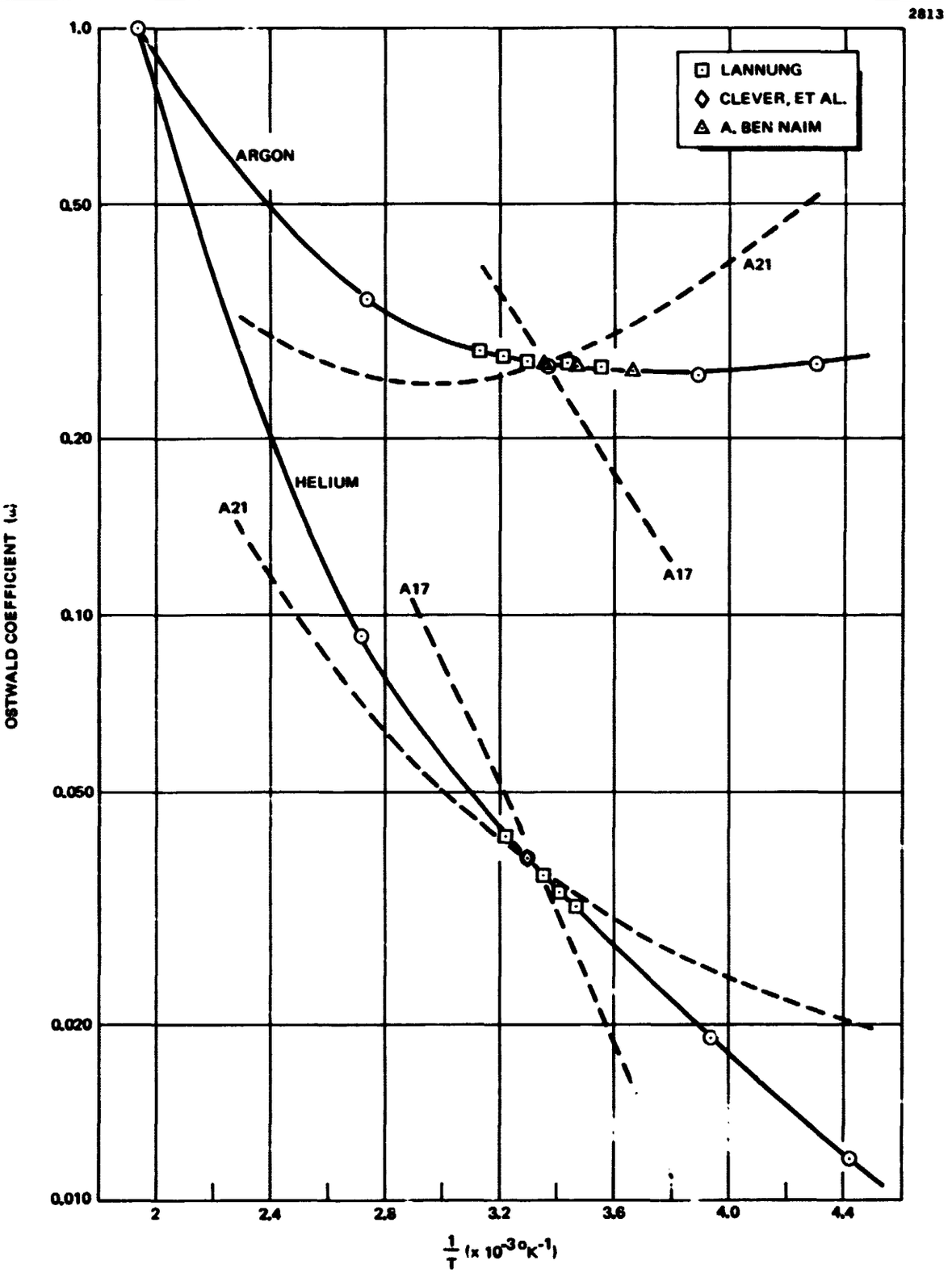

Figure A-2. Solubility of Helium and Argon in Methanol Compared with Theory

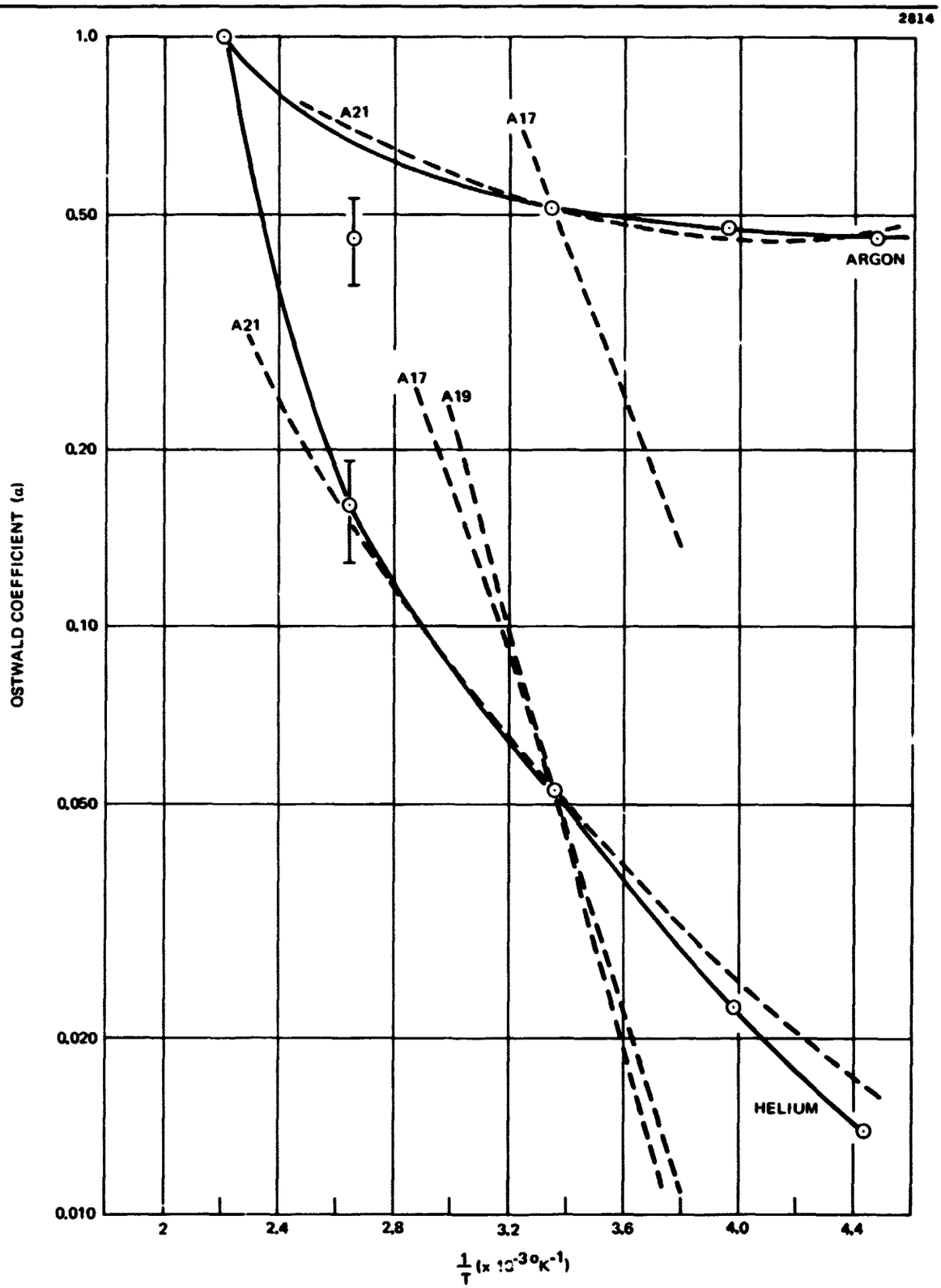

Figure A-3. Solubility of Helium and Argon in Freon-21 Compared with Theory

properties common to both gas dissolution and general heat pipe performance. The Ostwald coefficient of a gas is exponentially dependent on the solute and solvent molecular radiuses, and at 25°C, is exponentially dependent on surface tension. Solubility parameter theory also links the solubilities exponentially with latent heat of vaporization, as shown by the factor δ in Table A-1. For venting gas occlusions, it is desirable to have a high solubility, and therefore, the working fluid should have low surface tension and low h_{fg}, and the control gas, if any, should be a species with large molecular diameter.

The first requirement is in conflict with thermal performance of the heat pipe, and in conflict, to some degree, with the capability for venting, because a high surface tension pressure is desirable to increase the concentration gradient into the liquid surrounding a gas occlusion, thereby decreasing vent time. However, the use of a large diameter molecular species as control gas has no apparent drawbacks.

In addition to high solubility, a larger molecule has a lower gas-gas diffusivity, sharpening the diffusion profile in the heat pipe condenser. Futhermore, there is an apparent relationship between molecular diameter and the temperature coefficient of solubility for organic fluids. As shown in Section 4.1, the solubility temperature coefficient for argon in Freon-21 and methanol is much less than the temperature coefficient for helium in Freon-21 and methanol. This difference in behavior may be critical for applications where the system suffers large temperature excursions, because it is possible that the helium gas could precipitate out of solution as gas bubbles in an arterial passage or elsewhere.

A.11 REFERENCES

A1. J. Jolley, and J. Hildebrand, J. Am. Chem. Soc., 80, 1050 (1958).

A2. W.F. Linke, D. Von Nostrand, Solubilities, Princeton, N.J., 1958.

A3. J. Hildebrand and R. Scott, The Solubility of Nonelectrolytes, Dover Publications, 1964.

A4. D. Von Nostrand, Textbook of Physical Chemistry, Glasstone, New York, 1946.

A5. J.H. Dymond, J. Phys. Chem., 71, 1829 (1967).

A6. R. Linford and J. Hildebrand, J. Phys. Chem., 73, 4410 (1969).

A7. A. Ben Naim, J. Phys, Chem., 72, 2298 (1968).

A8. Handbook of Chemistry and Physics, 43rd edition, Chemical Rubber Publishing Co., Cleveland, Ohio.

A9. Perry's Chemical Engineer's Handbook, Fourth edition, McGraw Hill.

A10. R. Wiebe and V. Gaddy, J. Am. Chem. Soc., 59, 1984 (1937).

A11. J. Gjaldbaek, E. Anderson, Acta. Chem. Scand., 8, 1938 (1954).

A12. A. Zakharova, et. al., Russ. J. Phys. Chem., 43, 413 (1969).

A13. A. Lannung, J. Am. Chem. Soc., 52, 68 (1930).

A14. J. Gjaldbaek, H. Niemann, Act. Chem. Scand., 12, 1015 (1958).

A15. G. Archer and J. Hildebrand, J. Phys, Chem., 67, 1830 (1963).

A16. A. Schulze, Z. Physik. Chem., 95, 257 (1920).

A17. R. Linford and J. Hildebrand, Trans. Var. Soc., 66, 577 (1970).

A18. H. Clever, J. Phys. Chem., 62, 375 (1958).

A19. E. Reed, J. Droher, Report LMEC-69-36, Liquid Metals Engineering Center, AEC Contract AT(1403)-700, (1970).

A20. J. McKelvey. Solid-State and Semiconductor Physics. Harper and Row, N.Y., 1966.

A21. Y Kobatake, B. Alder, J. Phys. Chem., 66, 645 (1962)

A22. R. Pierotti, J. Phys. Chem. 67, 1840 (1963).

A23. H. Reiss, et. al., J. Chem. Phys., 32, 119 (1960).

A24. U. Uhlig, J. Phys. Chem., 41, 1215 (1937).

A25. J. Hildebrand and R. Scott, The Solubility of Nonelectrolytes, Reinhold Publishing, N.Y. (1950).

A26. J. Hirschfelder and C. Curtiss, Molecular Theory of Gases and Liquids, John Wiley and Sons, 1965.

A27. R. Svehla, NASA Tech. Report R-132, Lewis Research Center (1962).

A28. R. Reid and T. Sherwood, The Properties of Gases and Liquids, McGraw-Hill, (1966).

A29. H. Andersen, et. al., J. Chem. Phys., 57, 2626 (1972).

A30. L. Yen and S. Woods, A.I.Ch. E.J., 12, 95 (1966).

Appendix B
DISSOLUTION OF AN ELONGATED BUBBLE

Bubble dissolution in an artery is assumed to be composed of two separable components, end-cap diffusion and radial diffusion. End-cap diffusion is treated as in Section 2.2, with the two hemispheres assumed to be equivalent to one spherical bubble diffusing into a semi-infinite media. The initial radial time-dependent mass loss is described with a Fourier series solution, and the steady-state mass transfer is expressed with the familar logarithmic expression for diffusion through a thick-walled tube. The fluid surrounding the bubble is initially assumed in equilibrium with the general gas concentration in the vapor space, C_∞.

The initial dissolution of gas radially is exactly described by a Bessel function solution, but if the arterial wall is treated as a slab of thickness Δr, then the appropriate Fourier series solution, mathematically simpler, is a good approximation to the non-steady-state component of venting.

If the origin of the y-coordinate system is fixed to the inner wall of the artery and continued radially to the outer wall where $y = \Delta r$, then at $t = 0$, the inner wall, which was in equilibrium with the bulk fluid with $C = C_i$, is in contact with a gas mass producing a surface concentration $C = C_s$. Diffusion of gas from the interior now occurs. To account for the effect on diffusion of the screen or other porous media comprizing the artery wall, an effective diffusion coefficient D' is defined, where $D' = \lambda D$, and λ is a so-called tortuosity factor.

By the method of separation of variables, the one-dimensional solution to Fick's second law of diffusion is expressible as a Fourier series as

$$C(x, t) = (C_s - C_i)\left[(1 - y/\Delta r) - \frac{2}{\pi}\sum_{N=1}^{\infty}\frac{1}{N}\sin(N\pi\, y/\Delta r)\exp\left(-\left(\frac{n\pi}{\Delta r}\right)^2 D't\right)\right] \quad (B1)$$

The general technique used to obtain this solution is discussed in Reference B1. The quantity $(1 - y/\Delta r)$ is the steady-state solute distribution in a slab. If this component is neglected, the time-dependent diffusion is given by $D \cdot \partial c/\partial y$ at $y = 0$. The steady-state diffusion solution for concentric cylinders can be added to the non-steady-state component to obtain a good approximation to the exact radial solution,

$$\dot{m} = D'(C_s - C_i)\left[\frac{1}{R_a \ln\left(1+\frac{\Delta r}{R_a}\right)} + \frac{2}{\Delta r}\sum_{n=1}^{\infty} \exp\left[-\left(\frac{n\pi}{\Delta r}\right)^2 D't\right]\right] \quad \text{(B2)}$$

The total mass loss from the elongated bubble is obtained from the sum of Equation B2 over the area ℓ_o in length, and from the solution for diffusion from a constant diameter sphere, to account for end-cap loss. Translated to a decrease in length ℓ_o,

$$\frac{d\ell}{dt} = \frac{-2\alpha D'(C_g - C_\infty)}{C_g}\left[\left(\frac{1}{R_a \ln\left(1+\frac{\Delta r}{R_a}\right)} + \frac{2\Sigma}{\Delta r}\right)\frac{\ell}{R_a} + \frac{2\beta}{\lambda}\left(\frac{1}{R_a} + \frac{1}{(\pi Dt)^{1/2}}\right)\right] \quad \text{(B3)}$$

where Σ is an abbreviation for the summation given in (B2), C_g is the gas concentration in the gas occlusion, C_∞ is the gas concentration external to the artery, and β is a factor that corrects for the semi-infinite fluid plugs each hemispherical end cap diffuses into. The proper value for β, from experimental venting data, is discussed in Section 4.2.

In many cases, the time-dependent components in the collapse equation B3 could be neglected, giving

$$\frac{d\ell}{dt} = -2\alpha D'(1-f)\left[\frac{\ell}{R_a^2 \ln\left(1+\frac{\Delta r}{R_a}\right)} + \frac{2\beta}{\lambda R_a}\right] \quad \text{(B4)}$$

Integrated from $\ell = \ell_o$ to $\ell = 0$, the time to vent down to a spherical bubble is

$$t_l = \frac{R_a^2 \ln\left(1 + \frac{\Delta r}{R_a}\right)}{2 \alpha D (1-F)} \ln\left(1 + \frac{\lambda \ell_o}{2\beta R_a \ln\left(1 + \frac{\Delta r}{R_a}\right)}\right) \quad \text{(B5)}$$

REFERENCE

B1. R. V. Churchill, Fourier Series and Boundary Value Problems, McGraw-Hill, New York (1967).

Appendix C
DISSOLUTION OF AN ARTERIAL BUBBLE IN FLOW

Reference C1 presents empirical equations describing average unit-surface conductance for spheres and cylinders heated or cooled in liquid flow. The average unit-surface conductance of a sphere in flow is very close to the value obtained if the sphere is assumed constructed of an infinite number of cylindrical strips, each strip having the unit-area average conductance of a cylinder of radius R sin ϕ, where ϕ is the polar angle of the sphere.

In this condition, it is postulated that a small bubble rests, in gravity, at the top of the tubular artery. If the bubble is relatively small, the flow pattern seen by the bubble is very similar topologically to that seen by a bubble resting against a flat surface if there is an appropriate parabolic velocity profile relative to that surface. It is further theorized that the technique of dividing a sphere into incremental strips, and integrating local cylindrical conductance is again appropriate, but with the parabolic velocity distribution also factored in. Both the cylindrical and spherical conductances are square-root dependences on velocity and radius so that, from a practical standpoint, the system is somewhat forgiving of oversimplifications. The thermal conductance obtained is easily transformed to the mass transfer analog.

Proceeding as outlined, the average unit-surface conductance for a sphere in arterial parabolic flow is approximately

$$\frac{Q}{KA\Delta T} \cong \frac{1}{R_b} + \frac{0.792}{R_a}\left(\frac{Re}{8}\right)^{1/2}\left(P_r\right)^{1/3}\int_o^{\pi}\left[\sin\theta - \sin\theta\cos\theta\right]^{1/2} d\theta, \quad (C1)$$

where Re is the Reynolds number for flow in the artery, R_b is the instantaneous bubble radius, and $R_b \leq 1/2\ R_a$. In terms of the mass-transfer analog,

$$\frac{\dot{m}}{DA(C_s - C_i)} = \frac{1}{R_b} + 0.622\left(\frac{Re}{R_a}\right)^{1/2}\left(\frac{\mu}{\rho D}\right)^{1/3} \qquad \text{(C2)}$$

Substitution of this expression into dissolution Equation 26, neglecting the non-steady-state term $(1/\pi t)^{1/2}$, gives

$$\frac{dR}{dt} = \frac{-\alpha(GR + \delta)}{(R + 2/3\delta)}\left[\frac{1}{R} + B\right], \qquad \text{(C3)}$$

where B is a flow parameter given by

$$B = 0.622\left(\frac{R_c}{R_a}\right)\sqrt{Re}\,(Sc)^{1/3} \qquad \text{(C4)}$$

where Sc is the Schmidt number. Expression C3 can be integrated formally, but the resulting equation has such a complex form that no insight is gained into the dissolution process. One simple solution to Equation C3, where surface tension pressure dominates, is discussed in Section 2.5. Many other partial solutions are possible, depending on system conditions.

REFERENCE

C1. F. Kreith, Principles of Heat Transfer, International Textbook Co., Scranton, Penn. (1967).

G